(18) ARO 16010.1-A-E

(19)

(12)

AD A078587

LEVEL II

FINAL ~~ANNUAL~~ REPORT

(June 1978-August 1979)

FLUID AND THERMODYNAMIC CHARACTERISTICS OF COMPRESSIBLE RECOIL MECHANISM

(DAAG 29-78-G-0120)

submitted to

U.S. Army Research Office
Research Triangle Park
North Carolina 27709

U.S. Army Armament Research
and Development Command
Dover, New Jersey 07801

by

Ching Jen Chen Enzo O. Macagno

Energy Division and Iowa Institute of Hydraulic Research
College of Engineering
The University of Iowa
Iowa City, Iowa 52242

188300

(11) Aug 1979

(12) 80

79-12 27 130

188 300

FOREWARD

This report is the annual report of the research project entitled "Fluid and Thermodynamic Characteristics of Compressible Recoil Mechanism" covering the period from June, 1978 to August, 1979. The project originally was funded on February 1, 1977 for a three year period of research by the U. S. Army Weapon Command of Rhode Island, Illinois. However, the project was interrupted after the first year on February 1, 1978 because of the reorganization of the U. S. Army Armament Research and Development Command. The project was then reactivated by the U. S. Army Armament Research and Development Command from Dover, N. J. through U. S. Army Research Offices in North Carolina under the contract DAAG 29-78-G-0120 under a reduced funding level at approximately a one-half budget for the period from June, 1978, to August, 1979. The research effort thus is accordingly also reduced. The portion of the proposed experimental investigation was thus terminated and the effort is concentrated in the development of the numerical prediction for the fluid motion in the recoil mechanism. Substantial progress has been made in the numerical solution to the Navier-Stokes equation at high Reynolds number from the development of the new numerical scheme called "Finite Differential Method". An outline of the procedure of applying the method to the recoil mechanism is given which can be carried out in the third year effort.

The project was conducted by Professors C. J. Chen and E. O. Macagno with graduate research assistants N. H. Naseri-Neshat and A. M. Fard-Behbahani.

Table of Contents

List of Figures

List of Tables

Unclassified

SECURITY CLASSIFICATION OF THIS PAGE (When Data Entered)

REPORT DOCUMENTATION PAGE		READ INSTRUCTIONS BEFORE COMPLETING FORM
1. REPORT NUMBER	2. GOVT ACCESSION NO.	3. RECIPIENT'S CATALOG NUMBER
4. TITLE (and Subtitle) Fluid and Thermodynamic Characteristics of Compressible Recoil Mechanism		5. TYPE OF REPORT & PERIOD COVERED ~~Fluid~~ Report FINAL 6. PERFORMING ORG. REPORT NUMBER
7. AUTHOR(s) Ching-Jen Chen, Enzo O. Macagno		8. CONTRACT OR GRANT NUMBER(s) DAAG 29-78-G-0120 new
9. PERFORMING ORGANIZATION NAME AND ADDRESS Energy Division and Iowa Institute of Hydraulic Research, The University of Iowa, Iowa City, Iowa 52242		10. PROGRAM ELEMENT, PROJECT, TASK AREA & WORK UNIT NUMBERS NA
11. CONTROLLING OFFICE NAME AND ADDRESS U. S. Army Research Office Post Office Box 12211 Research Triangle Park, NC 27709		12. REPORT DATE August 1979 13. NUMBER OF PAGES 79
14. MONITORING AGENCY NAME & ADDRESS(if different from Controlling Office)		15. SECURITY CLASS. (of this report) Unclassified 15a. DECLASSIFICATION/DOWNGRADING SCHEDULE

16. DISTRIBUTION STATEMENT (of this Report)

Approved for public release; distribution unlimited.

17. DISTRIBUTION STATEMENT (of the abstract entered in Block 20, if different from Report)

NA

18. SUPPLEMENTARY NOTES

The view, opinions, and/or findings contained in this report are those of the author(s) and should not be construed as an official department of the Army position, policy, or decision unless so designated by other documentation.

19. KEY WORDS (Continue on reverse side if necessary and identify by block number)

Fluid flow, Reoil mechanisms, Numerical prediction, orifice flow.

20. ABSTRACT (Continue on reverse side if necessary and identify by block number) Fluid dynamic aspect of recoil mechanisms is studied with simple one dimensional analysis as well as two dimensional numerical analysis. Method and procedure for experimental simulation is given. Full scale and reduced scale simulation is analyzed for its advantages and disadvantages. A new numerical scheme called "finite differential" method is developed to solve the two dimensional unsteady Navier-Stokes equation. The new method utilizes the local analytical solution of the total problem. The solution of the problem is obtained by assembling the local analytic solution. The method is shown to be capable of solving flows with high Reynolds numbers.

DD FORM 1 JAN 73 1473 EDITION OF 1 NOV 65 IS OBSOLETE

Unclassified

I. INTRODUCTION

The recoil mechanism is a component of the recoil system which provides a retarding force acting on the gun so as to brake the rearward motion in the firing cycle. The counter-recoil mechanism is also a component of the recoil mechanisms which stores the energy during the recoil and dispenses it during the counter-recoil phase so as to bring the gun back into its in-battery position. Without a recoil system, the force acting on the gun and its mounts induced by firing the charge is so large that damages to the gun often immediately result. An improperly designed recoil mechanism can also affect the accuracy of the gun in hitting the target and reduce the life of the gun. Therefore, the recoil system is one of the most important components of a gun system.

Frequent failure and the undesirable characteristic of many springs used in the recoil mechanism prompted recent designers of a gun system to adopt more fluid-type recoil mechanisms (hydropneumatic) or the combination of fluid and spring type recoil mechanisms (hydrospring). The fluid recoil mechanism, gas or liquids, is throttling during a firing cycle through an orifice which divides the recoil mechanism into two or more chambers. The difference in the pressure between the chambers thus provides the retarding force for braking action. The retarding force and the counter-recoiling force are thus functions of the fluid motion, the type of fluids, and the orifice geometry of recoil mechanisms. Therefore, the knowledge of fluid mechanics of the recoil mechanism is an indispensable part of the weapon design.

The fluid type of record mechanism was considered in the 1960's by

the Rock Island Arsenal and the Iowa Institute of Hydraulic Research [1-5]. However, it was found [4] that the designed recoil characteristic such as retarding force and recoiling motion often do not agree with the experimental measurement. The reason for this discrepancy is largely due to lack of detailed knowledge about the fluid dynamic characteristics of the recoil mechanisms. In particular, the value of the orifice discharge coefficient which determines the flow rate through the orifice and, hence, the retarding force during recoil motion. The value of the orifice discharge coefficient in many designs was assumed to be constants, typically ranging from 0.6 to 0.9, which were obtained from experiments of steady flow through stationary orifice. However, the unsteady flow in the recoil mechanisms is created by the unsteady motion of the orifice. Indeed, the orifice discharge coefficient should be the orifice discharge function and should depend on the flow velocity and the location and geometry of the orifice.

Several experimental data for simple geometry and steady flow through stationary orifice are available [6]. Theoretically calculated orifice discharge coefficient for small Reynolds number with stationary orifice are also available [7]. However, neither experimental data nor theoretical prediction of the orifice coefficient are available for the moving orifice in unsteady flow with large Reynolds number such as in recoil mechanisms.

The aim of this project is to provide the fundamental description of fluid mechanics for recoil mechanisms and to present an approximate determination of orifice coefficient and to describe the fluid motion in the recoil mechanism.

II. ONE DIMENSIONAL ANALYSIS OF ORIFICE AREA AND ORIFICE DISCHARGE COEFFICIENT

In order to examine how the fluid flow in the record mechanism affect the record motion and how the orifice area is designed, a one dimensional analysis of fluid motion in the record mechanism is presented here.

II-1. Criterion of Orifice Design

A recoil mechanism may be designed to operate on incompressible or compressible principle. For incompressible type, the total volume of the recoil cylinder will remain the same during recoil motion since the fluid is treated as incompressible. For the compressible type, the volume may be decreased in the recoil motion. The fluid used in the recoil mechanisms may be gas or liquid such as air, nitrogen, hydraulic or silicone oil. In both cases, the orifice must be properly designed to achieve desired characteristics of retarding force for recoil mechanism.

Before one calculates the fluid motion and the pressure distribution in a recoil mechanism, design characteristics of recoil mechanisms should be first defined so that the required geometry of the orifice can be determined accordingly.

Generally, all recoil mechanisms work on some combination of the same basic principles; that of providing a controlled resistance over a set distance to check the motion of the recoiling parts, then returning them to the firing position and providing a sufficient restraint to hold them in that position at a given elevation. A basic requirement for a recoil mechanism is that the resistance to recoil should be nearly constant for a prescribed recoil distance, since this will produce the smallest possible force on the gun structure. A typical recoil force

versus recoil distance relation is given in Fig. 1. The area under the recoil force-time curve represents recoil impulse to be dissipated by the recoil mechanism. Clearly, a rectangular curve will yield the lowest retarding force for a given recoil motion. However, a rectangular curve is not applicable at the beginning because the recoil resistance K(t) should not exceed the recoil force B(t) created by the propellant gas.

The total resistance force K(t) is a combination of a hydraulic force $F_o(t)$, a spring force if a spring is used with fluid and friction of moving mechanism. Whichever the type of recoil mechanism is used, this force works as a unit.

In general, the recoil force B(t) is offset largely by the hydraulic resistance $F_o(t)$ offered by throttling the fluid through the controlling orifice and by the spring force. Thus, design of the control orifice is a vital part of the recoil mechanisms.

We now consider a basic recoil mechanism as shown in Fig. 2 that a recoiling mass M is subjected to a time dependent recoil force, B(t), from the discharge in the breech of a gun creating an acceleration of $\ddot{X}$ in the x direction. Here X = 0 is taken as the orifice plane before the recoil motion. The recoil motion of mass M forces the fluid to flow from Chamber (1) to Chamber (2). The orifice installed between the two chambers restricts the flow from Chamber (1) to (2) so as to create a pressure difference between the two chambers. This differential pressure acts on the wall of recoiling orifice A_1 and A_2 to control the recoiling speed and motion. The force balance for the recoil motion can be written as

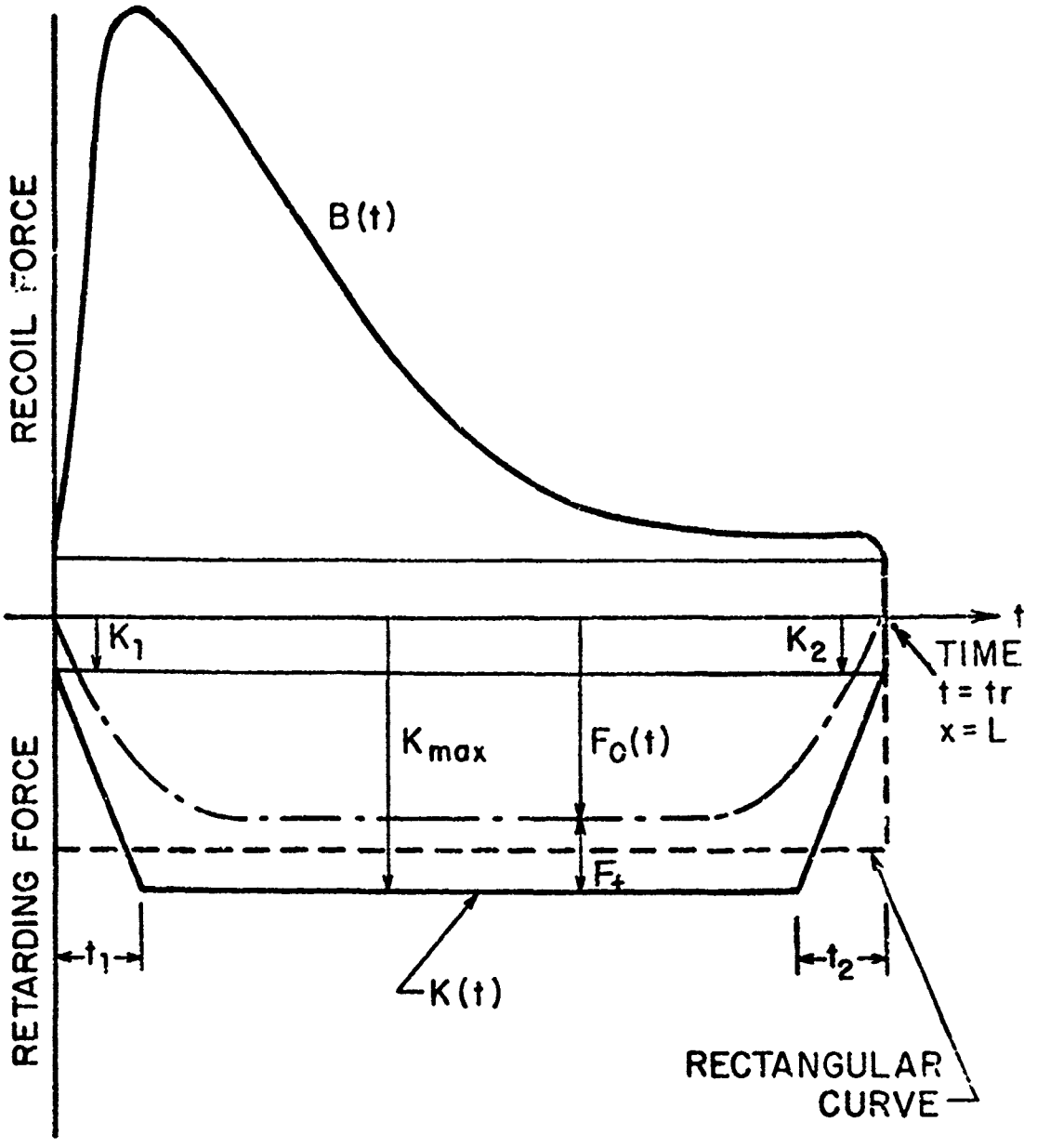

Figure 1. Recoil Force and Retarding Force of Recoil Mechanisms

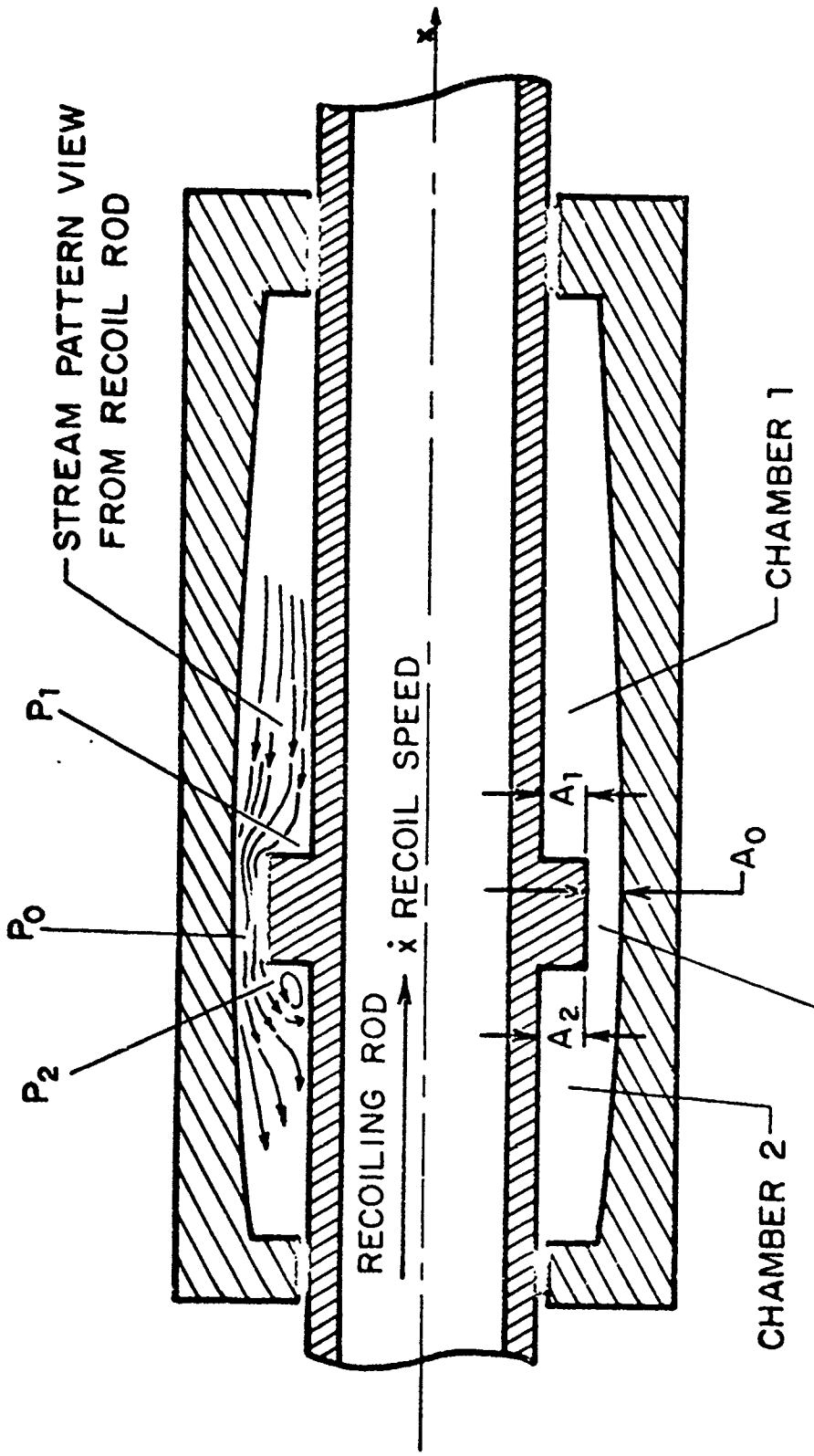

Figure 2. Typical Recoil Mechanism

$$\ddot{MX} = B(t) - K(t) + M\,g\,\sin\theta$$

$$K(t) = \int_{A_1} P_1 dA_1 - \int_{A_2} P_2 dA_2 + F_f = F_o(t) + F_f \qquad (2\text{-}1)$$

where P_1 and P_2 are respectively the pressure distributed on the orifice surface facing Chamber (1) and Chamber (2). A_1 and A_2 are area of the orifice facing Chambers (1) and (2). Here $A_1 = A_2$ is for incompressible type and $A_1 > A_2$ for compressible type. F_f is the frictional resistance force from seal, various moving parts and, if any, recuperator. The last term of Eq. (2-1) is the contribution of the gravitational force with θ being the inclined angle of the recoil mechanism with respect to horizontal plane. The dot on X denotes the time derivative. In Eq. (2-1), the mass M, the retarding force from breech B(t), two areas A_1 and A_2 and frictional resistance force, F_f, are assumed known but distribution of pressures P_1 and P_2 acting on the surface A_1 and A_2 are unknown and must be solved associated with the fluid motion induced by the motion of recoiling parts. In general, both P_1 and P_2 must be integrated from the pressure distribution respectively on their surfaces A_1 and A_2.

Now the pressure distribution on the orifice surface and their time variations must be determined by solving the fluid motion in the recoil fluid chambers. This creates the coupling between the recoiling force and the fluid motion. It should also be pointed out here that the designer has very little control over the resistance force, F_f, from the friction and recuperator and the gravitational force, M_g, but he can control the resistance offered by the pressure force from the two chambers by properly designing the orifice such that the total resistance to the

recoil force is sufficient to arrest the rearward motion of the gun in a specific recoil length allowed in the design.

One is now faced with the question of what orifice design will provide the lowest peak resistance force for a given mechanism. To set up the criterion for the orifice design, let us consider Eq. (2-1) for recoil motion again. K(t) is the total resistance force including frictional forces F_f and pressure forces F_o created from the fluid throttling through the orifice. As the design characteristic of recoil mechanisms required that the total resistance K(t) to recoil should be nearly constant for a prescribed recoil length, a trapezoidal shape for K(t) such as in Fig. 1 is normally adopted.

Since Eq. (2-1) is a second order ordinary differential equation, one needs two initial conditions to obtain a unique solution. These two may be taken as

$$t = 0 \qquad X = 0 \tag{2-2}$$

$$t = 0 \qquad \dot{X} = 0 \tag{2-3}$$

That is initially the recoil mechanism is at rest. However, if the total resistance K(t) is not specified, there will be infinite many solutions of X(t) to Eqs. (2-1), (2-2) and (2-3). To determine K(t), we need additional design constraints. They are:

(1) the velocity of recoil $\dot{X}$ is zero at the end of the recoil, $t = t_r$, or

$$t = t_r \qquad \dot{X}(t_r) = 0 \tag{2-4}$$

(2) the total length of recoil allowed is L, which must be achieved in a duration of t_r, or

$$t = t_r \qquad X(t_r) = L \tag{2-5}$$

While the recoil length may normally be specified, the time duration, t_r, to arrest the rearward motion of the recoil is dictated by the resistance force K(t) and is not known normally a priori. Indeed, t_r must be solved with K(t) together. To determine the function K(t) we reason as follows

First, at the beginning of recoil, t = 0, and at the end of recoil, $t = t_r$, the mechanism is at rest and zero acceleration $\dot{X} = \ddot{X} = 0$ and meantime the breech force is zero or $B(0) = B(t_r) = 0$. We thus require from Eq. (2-1)

$$K_1 = K(0) = Mg \sin \theta \tag{2-6}$$

$$K_2 = K(t_r) = Mg \sin \theta \tag{2-7}$$

Here K_1 and K_2 are the resistance at the beginning and at the end of recoil motion.

Secondly, integrating Eq. (2-2) twice and with the initial conditions (2-3) and (2-4), we obtain

$$M\dot{X} = \int_0^t B(t)\, dt - \int_0^t K(t)\, dt + Mg \sin \theta\, t \tag{2-8}$$

$$MX = \int_0^t \int_0^t B(\tau) d\tau dt - \int_0^t \int_0^t K(\tau) d\tau dt + Mg \sin \theta \frac{t^2}{2} \tag{2-9}$$

Now with additional design constraints (2-4) and (2-5), Eqs. (2-8) and (2-9) become

$$0 = \int_0^{t_r} B(t)dt - \int_0^{t_r} K(t)dt + Mg \sin\theta \; t_t \qquad (2\text{-}10)$$

and

$$ML = \int_0^{t_r} \int_0^{t} B(\tau)d\tau dt - \int_0^{t_r} \int_0^{t} K(\tau)d\tau dt + Mg \sin\theta \frac{t_r^2}{2} \qquad (2\text{-}11)$$

Integral Eqs. (2-10) and (2-11) thus provide us with a means of determining the recoil time duration t_r and the total resistance force K(t). Since the total resistance force K(t) is generally desired to be of trapezoidal shape as shown in Fig. 1, if the initial and final periods, t_1 and t_2, of the variable resistance force are specified then Eqs. (2-10) and (2-11) determine uniquely the time t_r and the maximum total resistance for K_{max}.

Either the moment area method or a trial-and-error procedure, as discussed by Arora and Haug [1] and Coberly [2], may be used to solve Eqs. (2-10) and (2-11). Readers are referred to the above references for more details. The total resistance function K(t) thus can be used as the criterion of orifice design.

When the total resistance function K(t) is determined one may substitute the K(t) function into Eqs. (2-8) and (2-9) to obtain the recoil velocity $\dot{X}(t)$ and the recoil displacement X(t) as a function of time. The recoil velocity and displacement in turn become the boundary conditions for the solution of fluid flow in the recoil mechanism. For the recoil mechanism shown in Fig. 2, the orifice now must move with $\dot{X}$ velocity in the recoiling phase.

The fluid throttling through the orifice must produce a resistance force such that when combined with other frictional resistance from

seals and other rubbing parts, F_f, it is equal to the desired total resistance force, K(t). It is a difficult task for a designer to design such an orifice, since he must solve or know how the pressure force is generated when the fluid is throttling through the orifice. What is more difficult, the orifice clearance area in general is variable at different locations; the flow is unsteady and may be in both laminar and turbulent regions.

II-2. Quasi-Steady One-Dimensional Solution

The fluid motion and the pressure distribution on the orifice surface are governed by the mass conservation equation, the equation of state, the Navier-Stokes equation and energy equation for unsteady compressible fluid. In principle, the continuity equation, momentum equation, equation of state and energy equation - total of six equations - provide the solution of pressure, density, temperature and three velocity components. These equations, however, are coupled with Eq. (2-1) through the moving boundary condition of X(t). Thus, the fluid motion must be solved with the piston moving at a speed of $\dot{X}(t)$.

The initial condition for the flow problem may be assumed to be at rest. Thus, the velocity is zero everywhere. The initial density and pressure in the recoil mechanism is uniform.

After the gun is fired, the boundary condition for the fluid motion required that the fluid on the recoil rod assumes the recoil velocity $\dot{X}(t)$ and is at rest on the stationary cylinder surface. Now the orifice cross section must be designed so that the pressure forces, F_o, created by the throttling of fluid between the two chambers plus other resistance

seals and other rubbing parts, F_f, it is equal to the desired total resistance force, K(t). It is a difficult task for a designer to design such an orifice, since he must solve or know how the pressure force is generated when the fluid is throttling through the orifice. What is more difficult, the orifice clearance area in general is variable at different locations; the flow is unsteady and may be in both laminar and turbulent regions.

II-2. Quasi-Steady One-Dimensional Solution

The fluid motion and the pressure distribution on the orifice surface are governed by the mass conservation equation, the equation of state, the Navier-Stokes equation and energy equation for unsteady compressible fluid. In principle, the continuity equation, momentum equation, equation of state and energy equation - total of six equations - provide the solution of pressure, density, temperature and three velocity components. These equations, however, are coupled with Eq. (2-1) through the moving boundary condition of X(t). Thus, the fluid motion must be solved with the piston moving at a speed of $\dot{X}(t)$.

The initial condition for the flow problem may be assumed to be at rest. Thus, the velocity is zero everywhere. The initial density and pressure in the recoil mechanism is uniform.

After the gun is fired, the boundary condition for the fluid motion required that the fluid on the recoil rod assumes the recoil velocity $\dot{X}(t)$ and is at rest on the stationary cylinder surface. Now the orifice cross section must be designed so that the pressure forces, F_o, created by the throttling of fluid between the two chambers plus other resistance

Forces, F_f, is equal to the required design characteristic of the total resistance force K(t). At present, no such general solution of fluid motion exists even for the simplest recoil mechanism.

We consider a simple fluid dynamic model for the recoil mechanism. This model in many applications does not provide an accurate description of the flow pattern in the recoil mechanism, but it provides the first approximate design of the control orifice. This method also provides a basis for further modifications in cases of complex geometries and compressible flow and the flow is one dimensional. The assumption of a quasi-steady flow is equivalent to the assumption that the flow is instantaneously steady and that the force due to the acceleration and deceleration of fluid in the recoil is negligible. The one dimensional assumption implies that the pressure is uniform in the radical section of the mechanism. The resistance force offered by the orifice in Eq. (2-1) thus may be written as

$$F_o(t) = K(t) - F_f = P_1A_1 - P_2A_2$$

For incompressible type of recoil mechanisms, we have $A_1 = A_2$ or

$$(P_1 - P_2) = F_o(t)/A_1 \tag{2-12}$$

The continuity equations for one-dimensional steady incompressible flow is approximately (see Figure 2)

$$A_oU_o = (A_1 + A_o)U_1 \tag{2-13}$$

Here A_o and A_1 are respectively the orifice clearance area and orifice surface area facing Chamber (1). U_1 is the average velocity in Chamber (1) relative to orifice velocity. From the boundary condition, we have

$$U_1 = \dot{X}(t) \tag{2-14}$$

The momentum equation under quasi-steady, one-dimensional assumption may be integrated from the Chamber (1) to the rear end of the orifice as

$$\frac{U_1^2}{2} + \frac{P_1}{\rho} = \frac{U_o^2}{2} + \frac{P_o}{\rho} + \Delta H_f \tag{2-15}$$

Where ΔH_f represents the loss of kinetic energy due to viscous friction and, if the flow becomes turbulent, turbulent shear. There are six unknowns, P_1, P_2, P_o, U_1, U_o, and A_o, in four Eqs. (2-12), (2-13), (2-14) and (2-15). To facilitate the solution for orifice clearance area A_o, we assume that the pressure P_2 on the rear orifice surface is approximately equal to the pressure at the end of orifice P_o or

$$P_2 \doteq P_o \tag{2-16}$$

The reason for adopting this approximation is as follows. As shown in Fig. 2, the one-dimensional approximation is perhaps invalid immediately behind the orifice because from experiments conducted by Chen et al. [7] as shown in Fig. 3, we recognized that the flow always separates at the rear side of orifice except at the start of recoil motion. Therefore, for one-dimensional assumption to remain valid at the end of orifice, the flow should be considered like a jet (see Fig. 3) and separates at the rear end corner of the orifice. Under this condition, the pressure in jet portion of the flow will remain approximately P_o. Thus, for no other means of determining the pressure on the rear surface of orifice, P_2, we equal P_2 to P_o on the same cross section which is the closest pressure available under one-dimensional assumption.

Furthermore, the loss of kinetic energy due to friction, ΔH_f, is normally proportional to the pressure difference $(P_1 - P_2)/\rho$ or

$$\Delta H_f \sim (P_1 - P_2)/\rho \tag{2-17}$$

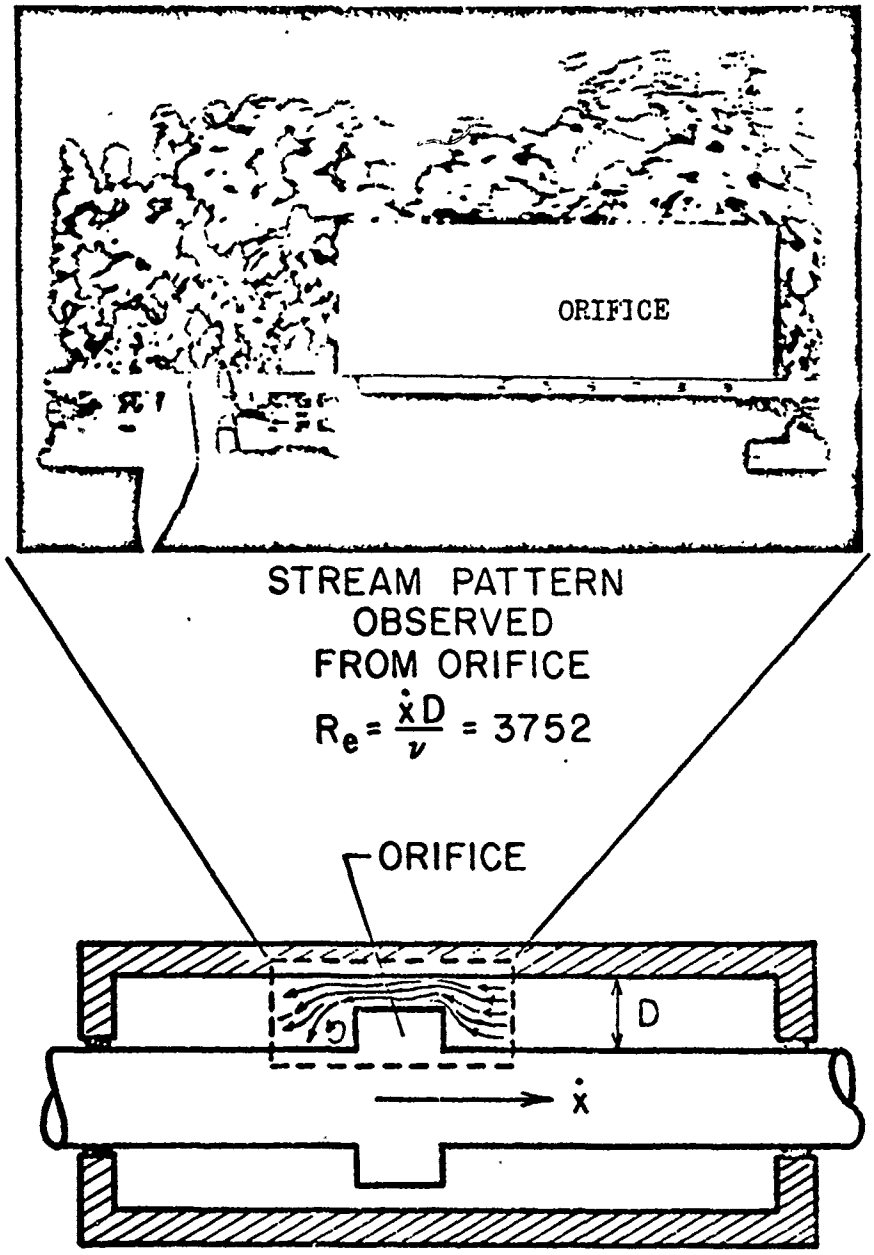

Figure 3. Flow Pattern Near Orifice

Thus, combining Eqs. (13), (14), (15), (16), the orifice velocity U_o can be written as

$$U_o = C_D \sqrt{2(P_1 - P_2) \Big/ \left[1 - \left(\frac{A_o}{A_1 + A_o}\right)^2\right] \rho} \qquad (2\text{-}18)$$

Here the orifice discharge coefficient C_D is introduced to account for the frictional loss and also to serve as a correction factor for the assumptions made, namely, one-dimensional quasi-steady flow and the assumptions that lead to Eqs. (2-16) and (2-17). More discussions on the coefficient C_D are given in Section IV.

Now from Eqs. (2-13) and (2-14) we also have

$$A_o = A_1 \Big/ \left(\frac{U_o}{\dot{X}} - 1\right) \qquad (2\text{-}19)$$

We thus can solve the orifice clearance area A_o from Eqs. (2-18), (2-19) and (2-12) as

$$\frac{A_o}{A_1} = \left[\sqrt{\frac{C_D^2}{\dot{X}^2} \frac{(P_1 - P_2)2}{\rho} + 1} - 1\right]^{-1}$$

or

$$\frac{A_o}{A_1} = \left[\sqrt{\frac{C_D^2 F_o(t)2}{\dot{X}^2 \rho A_1} + 1} - 1\right]^{-1} \qquad (2\text{-}20)$$

Equation (2-20) thus provides an approximate way of predicting the orifice clearance area for recoil mechanisms. It should be noted that the orifice area A_o is a function of orifice surface area A_1, recoiling speed $\dot{X}$, fluid density, ρ, orifice discharge coefficient, C_D, and the resistant force $F_o(t)$ required from the criterion established for the orifice design. Since both $F_o(t)$ and $\dot{X}$ are time dependent and the orifice moves with $\dot{X}$, the orifice area A_o must in general vary with the recoil distance X. The orifice area A_o can now be predicted if the orifice discharge coefficient C_D is known.

II-3. Orifice Discharge Coefficient C_D

The orifice discharge coefficient C_D was originally introduced to account for the pressure loss in a steady flow through an orifice. Customarily, it is treated as a constant. However, in case of recoil mechanisms C_D certainly is not a constant for the following reasons. First the recoil rod starts with zero speed and is accelerated to a high speed flow. Then it decelerates to zero speed and reverses the direction of motion in the counter-recoil motion. In the process, the flow starts from laminar motion to turbulent flow and then back to laminar motion again. The Reynolds number based on upstream gap and instantaneous average velocity may vary from zero to an order of 10^4. The orifice discharge coefficient certainly should vary since Reynolds number varies over such a wide range. In addition, in order to create a desirable characteristic of the recoil motion, the orifice clearance area A_o must be designed to vary. In summary, the orifice coefficient C_D should be dependent of:

A. Geometry of orifice and shape of Chambers (1) and (2).

B. Time variable.

C. Laminar and turbulent phenomena.

D. The average velocity across the orifice and viscosity and linear dimensions of orifice, or the Reynolds number.

E. Fluid compressibility.

The precise value of orifice discharge coefficient C_D for recoil mechanisms is not available to date since design of an orifice varys from one gun to another. Even for the same weapon, if a different charge is used, the orifice coefficient will be different because differenc recoil forces produce different recoiling speeds. Although as a rough approximation, constant values of C_D, between $0.7 \sim 0.9$, had been used [3, 4] but the resulting resistance forces were not satisfactory. In addition, the resistance force generated by the recoil mechanism was shown by Nerdahl and Frantz [5] and Coberly and Frantz [6] to be sensitive to the change of the value of orifice discharge coefficient. Therefore, a variable orifice discharge coefficient should be used whenever the variable value of C_D is available. To date neither experimental correlation nor theoretical prediction for variable C_D is yet available. Chen and Macagno [7] are currently attempting to solve the detail of fluid motion and thereby to predict the value of C_D from the numerically prediction pressure distribution. While the progress is being made, we suggest the following temporary measure. To determine the variable orifice discharge coefficient, we propose that the value of variable orifice discharge coefficient at any instance during the recoil be the value for steady flow with the flow Reynolds number , UD/ν, corresponding

to the instantaneous Reynolds number $\dot{X}D/\nu$. Here D is the upstream characteristic length, the diameter in case of tube flow and the gap width in case of annular flow. U is the average velocity upstream of the orifice. This assumption is consistant with the quasi-steady assumption made in deriving Eq. (2-21).

Figure 4 shows the experimental correlation [8] of the orifice discharge coefficient, C_D, versus steady flow Reynolds number UD/ν as defined by Eq. (2-18). In this case A_o is the orifice hole area $\pi d^2/4$ and $(A_1 + A_o)$ is the upstream area or $\pi D^2/4$. Although the geometry of orifice in Fig. 4 differs from the one in Fig. 2 for recoil mechanisms, Fig. 4 does illustrate the qualitative variation of orifice discharge coefficient with Reynolds number as well as the geometry. In Fig. 4, L is the thickness of the orifice. The ratio L/D seems to have an appreciable effect on C_D value. For a given Reynolds number C_D value in general increases with L/D ratio except at a large Reynolds number over 10^3.

The flow over Reynolds number of 10^3 is likely to be turbulent in some region of the flow. Turbulence is likely to be present near both orifice front and rear extruding corners and behind the orifice. The flow near the orifice is very complicated. The flow may separate at the front corner and reattach and then separate at the rear corner again. Even when the upstream slow is steady, the separation phenomena may still be unsteady. That is, the separation bubble may grow to a certain size and then separate from the corner and is carried downstream. A new separation bubble may follow to form at the front corner again and the phenomenon repeats to give a definite periodic separation. The

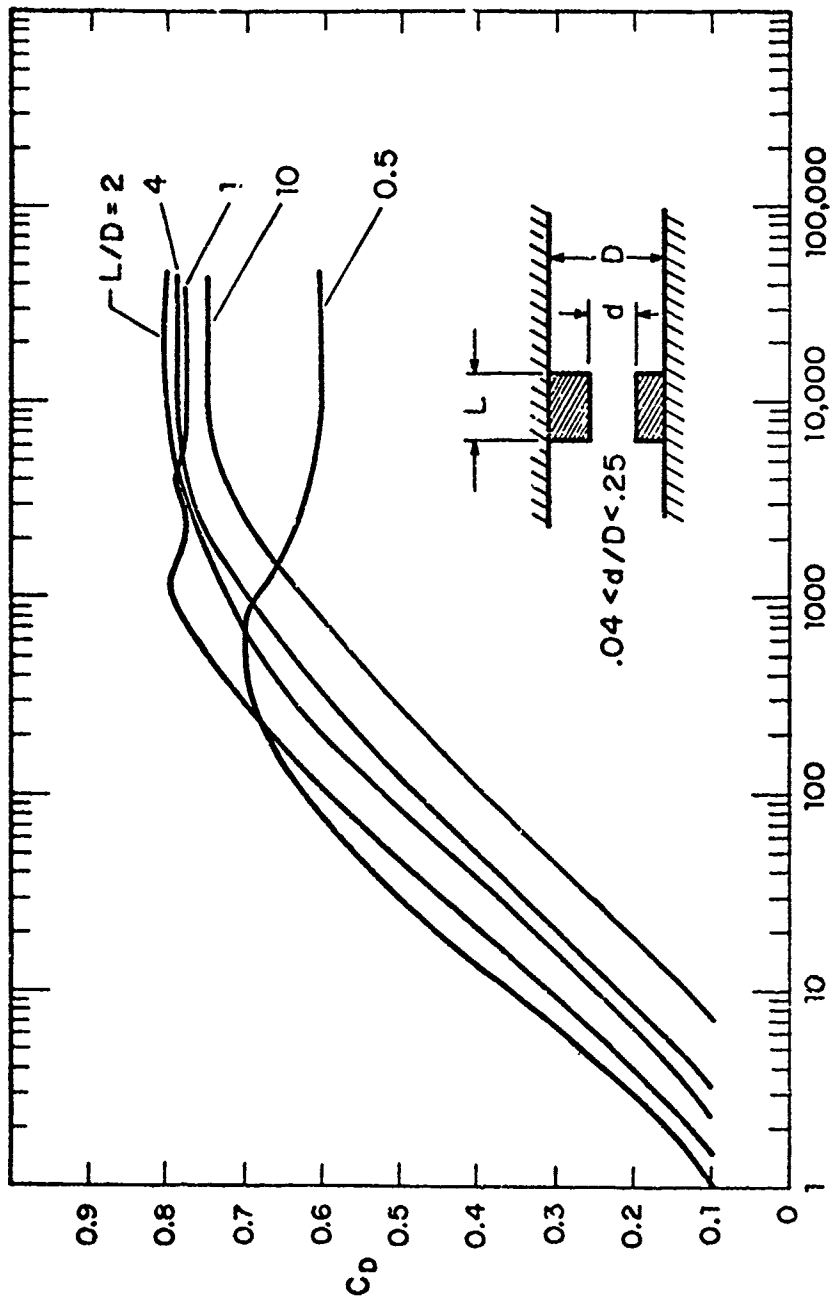

Figure 4. Orifice Coefficient vs. Reynolds Number

above mentioned phenomenon was observed by Chen and Macagno [7] in simulation of recoil motion with a similar configuration as shown in Fig. 3 at Reynolds number of 3752 based on upstream gap and velocity.

Examining Fig. 4, we may conclude that the orifice discharge coefficient C_D is less sensitive to the ratio of d/D in the range 0.04 to 0.25 than to the ratio of L/D. This has a favorable implication that the C_D is less dependent on the variable orifice clearance area A_o required in recoil mechanisms since the ratio $A_o/(A_o + A)$ is similar to $(d/D)^2$ in Fig. 4. This implication will lessen the complication in determining C_D for recoil mechanism. The variable orifice coefficient C_D to be used in recoil mechanism is then a strong function of instantaneous Reynolds number and the ratio of orifice thickness to the upstream gap or L/D.

When the fluid is compressible, the orifice coefficient should be modified. This is discussed also in the report by Chen and Macagno [7].

In summary, if the resistance force offered by recoil mechanism is defined, for example, a trapezoidal function in time, then a criterion for orifice design may be reduced from the equation of motion for recoil mechanism. The orifice clearance area A_o may then be approximately predicted from the quasi-steady one dimensional analysis for incompressible flow. However, the orifice discharge coefficient, C_D, must be provided from experimental correlation. Since the orifice area, A_0, in general varies with recoil distance, a variable orifice discharge coefficient, C_D, is proposed and, as a temporary measure, is taken as that of the steady flow with the instantaneous Reynolds number XD/ν replacing the steady Reynolds number.

For future design of recoil mechanism, unsteady two dimensional analysis of flow motion is proposed so that detail and precise pressure distribution on both sides of the orifice surface may be predicted. Such an analysis may be made quite versatile in that orifice geometry, recoil speed and distance can all be made as input parameters.

III. SIMULATION OF FLUID DYNAMIC CHARACTERISTICS IN RECORD MECHANISM

In this section, we are concerned with the simulation of the fluid dynamics of recoil mechanisms so that the orifice discharge coefficient, the recoil motion and force may be properly predicted. In the simulation experiment, it may also be possible to study the flow patterns, and other informations which are helpful in understanding the dynamics of recoil systems. The possibility of using different media and materials in the simulation is examined. The design configuration is made for compressible fluid recoil mechanism, however, the design procedure may be applied to conventional recoil mechanisms. The immediate goal of the design is to obtain experimentally the orifice discharge coefficient. In the design, calculation of the discharge coefficient is accomplished through the measurement of forces that are imparted to the stationary and moving parts of the recoil mechanism, and the measurement of fluid pressure in the recoil mechanism. The simulation may be also used for comparison with the numerical predictions.

III-1. Simulation Analysis

The purpose of a recoil mechanism is to provide a retarding force acting on the recoiling parts of the gun in order to control the motion induced by firing the charge. Two types of recoil mechanisms for large caliber weapons are in use: (A) compressible fluid (hydropneumatic) type, and (B) spring-fluid (gas or liquid) type. The detailed description of recoil mechanisms are available in [9] and [10]. In the present simulation design, a single orifice, hydropneumatic without spring is considered. Figure (5) is a schematic sketch of such a recoil mechanism.

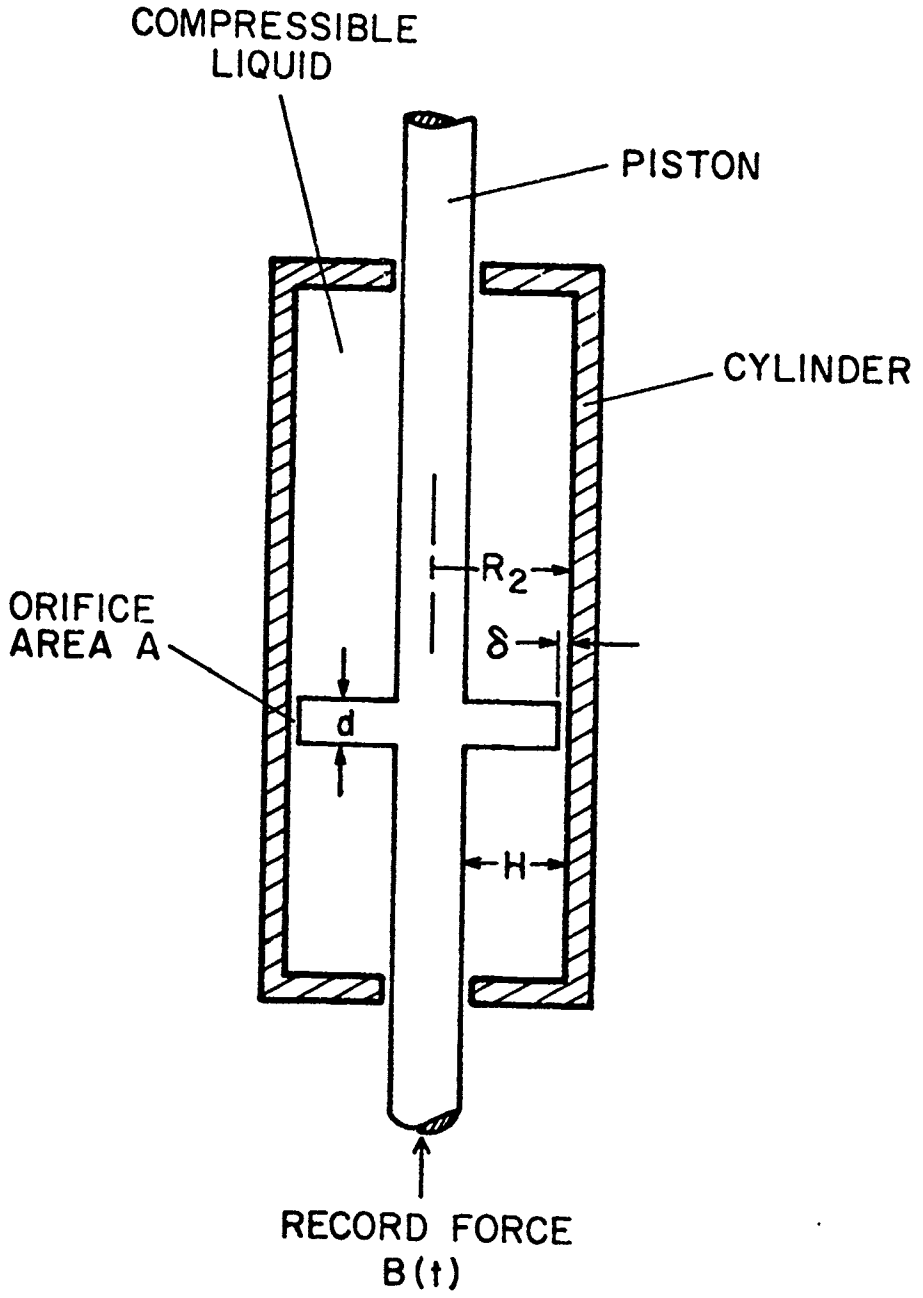

Figure 5. Typical Recoil Mechanism

In order to conduct a simulation experiment, the similarity parameters of recoil mechanism must be simulated. To achieve this, let us describe the similarity parameters by examining fluid flow and piston motion. The fluid and piston motions are governed separately by two different momentum equations. The two equations are not independent. They are coupled through the boundary conditions and pressure distribution on the wall surface. Therefore, in the simulation analysis, both fluid and solid momentum equations must be examined in addition to geometrical similarity. We examine these similarities in detail.

(A) Geometry Simulation: The geometric simulation can be carried out by taking the ratio of all corresponding lengths of prototype and simulated model equal to an arbitrary constant. Three dimensionless geometric parameters are considered necessary for simulation. They are the ratio of orifice gaps to the piston flange, δ/H (see Fig. 5), the width of the orifice to the piston flange (d/H), and the ratio of piston flange to the piston radius (H/R_2) or:

$$N_{G1} = \delta/H,\ N_{G2} = d/H,\ N_{G3} = H/R_2$$

(B) Fluid Dynamic Simulation: The fluid dynamic simulation of unsteady flows require two dimensionless similarity parameters which must be kept the same for both prototype and simulation design. These two similarity parameters are Reynolds number and Strouhal number. The definition of Reynolds and Strouhal number is obtained from the governing equation for the fluid flowing through the orifice. The Navier-Stokes equation for an unsteady, axisymmetric, laminar flow with constant physical properties and negligible body force is:

$$N_S \frac{\partial v_z}{\partial t} + v_z \frac{\partial v_z}{\partial z} + v_r \frac{\partial v_z}{\partial r} = - \frac{\partial p}{\partial z} + \frac{1}{Re}\left(\frac{\partial^2 v_z}{\partial z^2} + \frac{1}{r}\frac{\partial v_z}{\partial r} + \frac{\partial^2 v_z}{\partial r^2}\right) \qquad (3\text{-}1)$$

where

$$t = t^*/T,\ r = r^*/R_2,\ z = z^*/R_2,\ v_r = v_r^*/V,\ v_z = v_z^*/V,\ p = p^*/\rho^* v^2$$

where V and R_2 are the maximum piston velocity (reference velocity) and the cylinder inner radius as shown in Figure 5 (reference length), t^* denotes time, z^* and r^* axial and radial coordinates, v_z^* and v_r^* axial and radial components of velocity, and ρ^*, p^* and ν denote density, pressure, and kinematic viscosity, respectively. T is the reference time and can be taken as the period of the recoil motion. N_S and Re are Strouhal and Reynolds numbers, respectively or:

$$Re = \frac{vR_2}{\nu} \text{ and } N_S = \frac{R_2}{\nu\tau} \qquad (3\text{-}2)$$

Re and N_S are the two similarity parameters to be simulated in the design analysis.

(C) Piston's Motion Simulation: In order to have a complete simulation between the prototype and simulation model, it is obvious the similar piston's motions is needed for both cases. This is to say that the piston's displacement profile must be the same for the prototype as well as the simulation model. The governing equation for the motion of the piston is the Newton's second law, which can be written as:

$$m \frac{dv_p^*}{dt^*} = B_{(t)}^* - F_{(t)}^* \qquad (3\text{-}3)$$

where $B_{(t)}^*$ and $F_{(t)}^*$ denote the breech and retarding forces on the piston, respectively, and m is the recoil mass. v_p^* is the piston velocity and t^* is time. Equation (3-3) may be made dimensionless with the following expressions:

$$t = \frac{t^*}{\tau},\ v_p = \frac{V_p^*}{V},\ B'_{(t)} = \frac{B^*_{(t^*)}}{B},\ F'_{(t)} = \frac{F^*_{(t^*)}}{F}$$

where B and F are the maximum breech force and the maximum retarding force. Introducing the above expressions into (3-3)

$$\frac{dV_p}{dt} = N_B\ B'_{(t)} - N_F\ F'_{(t)} \tag{3-4}$$

The dimensionless parameters $N_B = \frac{B\tau}{mV}$ and $N_F = \frac{F\tau}{mV}$ must be the same for the simulation design to achieve the desired simulation. To facilitate the calculation of N_F and N_B, F will be calculated from the following equation:

$$F = \Delta p \times A \tag{3-5}$$

where Δp is the pressure difference on the two sides of the piston and A is the piston flange area. It should be remarked that equation (3-5) is the key equation for coupling fluid motion and piston motion. The value of the breech force B can be obtained from the recoil force that is generated by the propellant used in a particular recoil mechanism.

The goal of simulation experiment is to provide information about the fluid dynamic characteristics of recoil mechanisms, in particular the orifice discharge coefficient. To determine the orifice discharge coefficient in the simulation experiment, one may measure the force, F, that is on the recoil system stand and the recoil piston motion during the experiment. Through equation (3-5) the force measurement provides the amount of pressure exerted on the walls of the cylinder which in turn will be used to determine the orifice discharge coefficient C_D. The determination of the orifice discharge coefficient C_D, may be derived as follows: The momentum equation (3-2) with one dimensional approximation may be integrated along the stream line to give an

approximate formula as shown in Eq. (3-6) where ΔH is the energy loss due to viscous effect.

$$\frac{v'^2}{2g_c} + \frac{p'}{\rho} = \frac{v^2}{2g_c} = \frac{p}{\rho} - \Delta H \tag{3-6}$$

In equation (3-6) the flow is assumed to be quasi-steady and the coordinate system is fixed on the cylinder. ρ is the density of fluid and g_c is gravitational constant. p' and p are the averaged pressures downstream and upstream of the orifice, respectively. v and v' are the velocities at the upstream location and at the orifice, respectively. From continuity equation for the incompressible fluid, we have

$$Av = A'v' \tag{3-7}$$

where A and A' are the piston flange area and the orifice area, respectively. Combining equations (3-6) and (3-7), one obtains the fluid velocity at orifice area as:

$$v' = C_D\sqrt{\frac{\Delta p(2g_c)}{\rho}} \tag{3-8}$$

where C_D is introduced to account for the energy loss, unsteady flow and one dimensional approximation. The variables Δp, v', C_D and A' may be considered to vary with respect to time in the recoil system. From equations (3-8) and (3-7), it is obvious that if v, v', Δp, A and A' are known C_D may be calculated. For a simulation experiment A and A' are given. The fluid velocity at the orifice v' can be obtained from the measurement of piston velocity V through equation (3-17). The determination of the pressure difference Δp may be achieved by measuring the retarding force F on the cylinder with equation (3-5). The force F

can be measured such as by a strain gauge type of instrumentation with an experimental arrangement shown in Fig. (6). The piston velocity can be measured also during the experiment by displacement transducer. The force F can be obtained as follows: Suppose that the hydraulic fluid of the simulation model is evacuated such that inside the recoil system there is vacuum (or just air). Then the recoil motion of the piston will be met by only the frictional force from the seals of the outer cylinder and may be recorded as curve (a) in Fig. (7). Now, with the simulated hydraulic fluid filling the recoil mechanism, the recoil motion will be retarded by the additional force $F = \Delta p_* A$. This force F may then be obtained by subtracting the frictional force (curve a) from the force received by the external cylinder of curve (b) on Fig. (7). The difference between curve (a) and (b) is due to the force exerted by fluid on the orifice and hence the recoil mass. Once F is found, Δp can be calculated and, using equation (3-8), C_D can be plotted versus time.

III-2. Simulation Design

As stated previously, the present design of simulation experiment is for determination of orifice discharge coefficients in recoil mechanisms. In order to simulate the fluid flow in the recoil mechanism, the shape of the geometry and the geometrical ratios $N_{G1} = \delta/H$, $N_{G2} = d/H$, $N_{G3} = H/R$, Strouhal number N_S and Reynolds number, Re, must be simulated for both the prototype and the simulation model. In order to simulate the recoil motion, the parameters N_F and N_B must also be simulated for the prototype and the simulation design. Based on available date [10] N_S, R_e, N_F and N_B can be calculated for the prototype. One of the simulation

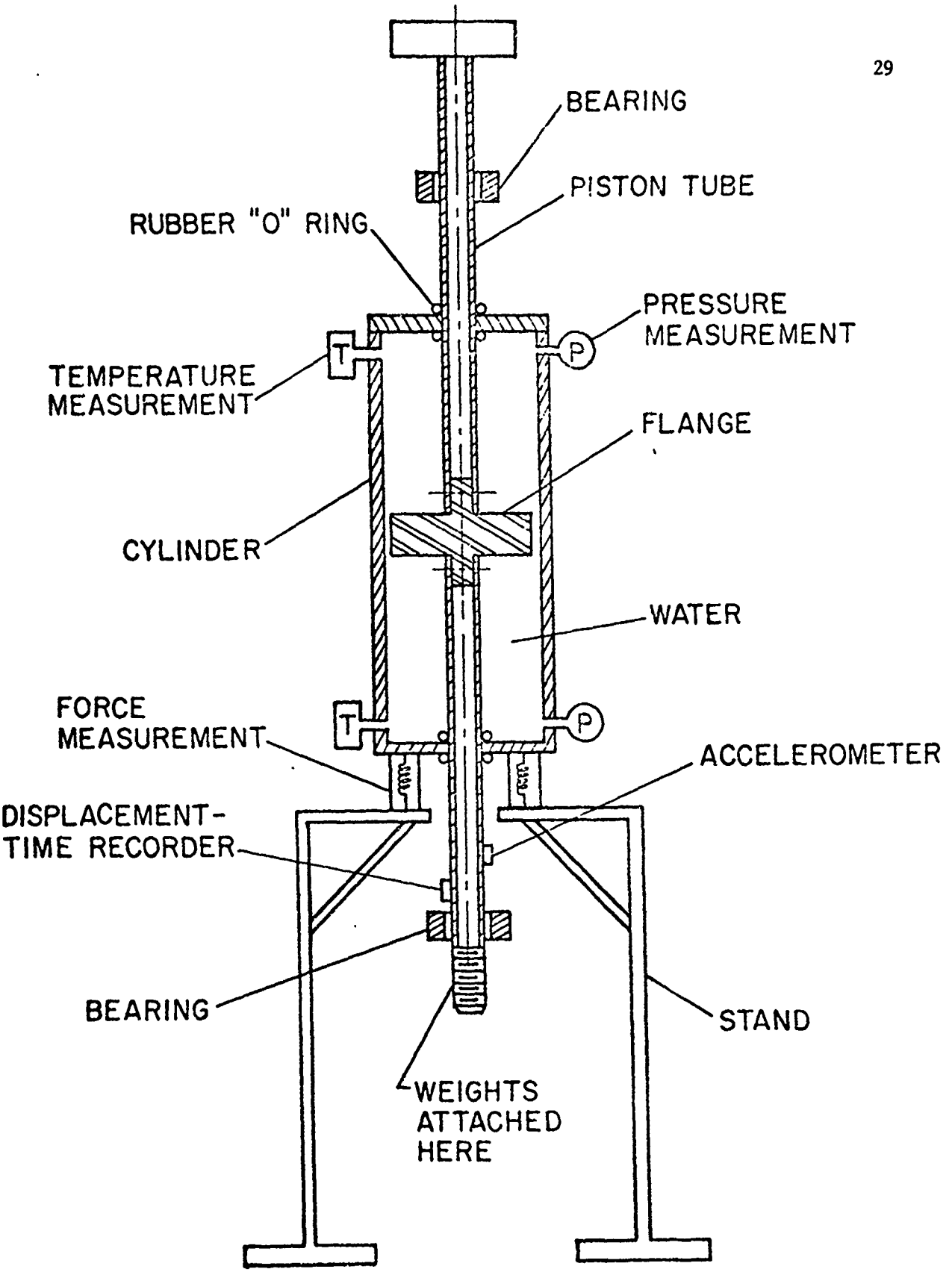

Figure 6. Design for Simulation Model (Schematic)

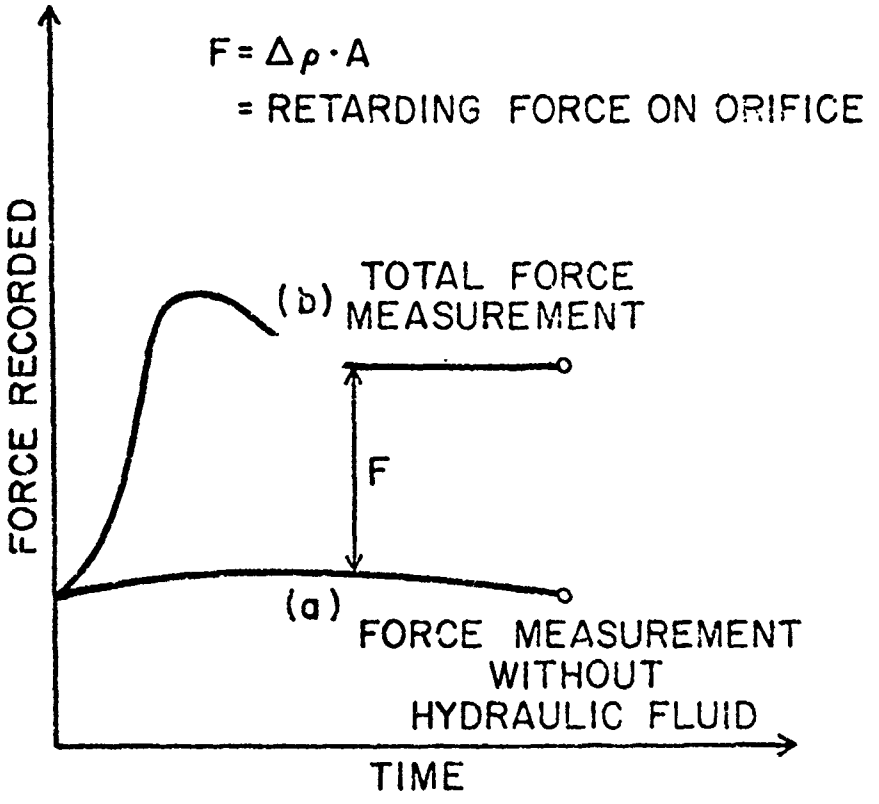

Figure 7. Force Recorder Plots

consideration is that the mass of the recoil piston in the simulation experiment should be reasonable. Another consideration is that the time duration of the experiment should be reasonably long to permit accurate measurements. Table 1 shows the properties of water and Dow Corning 210-10 centistoke silicone fluid. Table 2 shows the properties of "clear lucite" which can be used for the cylinder in the simulation. Clear lucite is a material strong enough to withstand the simulated stresses. It is transparent, allowing observation of fluid motion during the experiment.

In order to achieve the simulation, we choose the simulation fluid to be water which has a smaller kinematic viscosity (1.06×10^{-5} ft^2/sec) than the hydraulic oil(typically 10^{-4} ft^2/sec). The smaller the fluid kinematic viscosity is, the smaller the simulated piston velocity is required to achieve the same Reynolds number $\frac{VR_2}{\nu}$. This is good because it leads to a longer observation time for the simulation than that would be in the real recoil motion.

Consideration of using water provides many advantages in the simulation. In the following, we examine the use of water as the simulation fluid instead of the Dow Corning oil. Table 3 shows different parameters and symbols with their definition. These values are taken from [10] the recoil mechanism used in the simulation analysis. In the complete simulation, all geometry ratios $N_{G1} = \delta/H$, $N_{G2} = d/H$ and $N_{G3} = H/R_2$ must be kept similar. We now need to simulate geometric similarity N_{G1}, N_{G2}, N_{G3}, fluid flow similarity, N_S, Re and recoil similarity N_F and N_B. Table 4 gives the characteristic value of various simulation (see Fig. 5) where

TABLE 1. PROPERTIES OF FLUIDS

Dow Corning Silicone Fluid 210-10	
Specific gravity	0.94
Density (at STP)	0.03396 lbm/in^3
Coefficient of Thermal Expansion	0.006 in/m/°F at STd P.
Viscosity	10 centistoke
Power Point at St d Pressure	-85°F
Flash Point at St d Pressure	325°F
Specific Heat at 77°F	0.4 Bt/lbm °F
Boiling point at 0.5 mm Hg.	Absolute Pressure + 392°F
Water	
Specific gravity	1
Density (at STP)	0.036 lbm/in^3
Coefficient of Thermal Expansion	0.148 1/°R
Viscosity	1.42 Centipoise
Specific Heat at 77°F	0.99 Btu/lbm °F

TABLE 2. PROPERTIES OF CLEAR LUCITE

Specific Gravity	1.19
Tensile Strength	10500 (psi)
Flexural Strength	16000 (psi)
Compressive Strength	18000 (psi)
Modulus of Elasticity	45000 (psi)
Coefficient of Thermal Expansions	0.00005 (in/in°F)
Refractive Index	1.49

TABLE 3. LIST OF SIMULATION VALUES

Symbol	
R_2 = Cylinder inner radius	7 in
ν = Kinematic viscosity	1.07×10^{-4} ft^2/sec
v = Piston velocity	33.33 ft/sec
v' = Fluid velocity at orifice	558.735 ft/sec
A = Piston flange area	57.005 in^2
A' = Orifice area	4 in^2
τ = Period of a cycle	0.05 sec
m = recoil mass	2855 lbm
ρ = density	0.03396 lbm/in^3
g_c = gravity acceleration	32.2 lb.ft/lb. sec^2
F = Retarding force	391271.15 lb
B = Breech force	
N_S = Strouhal number ($R_2/v\tau$)	0.35
R_e = Reynolds number ($R_2 v/\nu$)	3046063
N_F = $F\tau/mv$	0.1935
D_1 = Piston outer diameter	10.25 in
δ = Orifice opening	0.09 in
H = Flange Height	1.775 in
d = Flange thickness	1 in
L = Cylinder length	18 in

TABLE 4 CHARACTERISTIC VALUE FOR SIMULATION DESIGN

	Recoil Mechanism Compressible Fluid	Fullsize Simulation (K = 1) Water	Complete Simulation (K = 0.357) Water
Cylinder length	18 in.	18 in.	6.5 in.
Flange thickness (d)	1 in.	1 in.	0.357 in.
Piston O.D. D_1	10.25 in.	10.25 in.	3.66 in.
Cylinder I.D. D_2	14 in.	14 in.	5 in.
Flange height H	1.775 in.	1.775 in.	0.634 in.
Orifice gap δ	0.08 in.	0.09 in.	0.053 in.
Piston length	50 in.	50 in.	17.85 in.
δ/H	0.0507	0.0507	0.0507
Piston Flange Area A'	67.055 $in.^2$	67.055 $in.^2$	8.614 $in.^2$
Average orifice Area A'	4 $in.^2$	4 $in.^2$	0.499 $in.^2$
Kinematic viscosity ν	1 07 x 10^{-4} ft^2/sec	1.06 x 10^{-5} ft^2/sec	1.06 x 10^{-5} ft^2/sec
Piston velocity v	33.33 ft/sec	3.30 ft/sec	9.245 ft/sec
Fluid velocity v'	558.735 ft/sec	55.35 ft/sec	159.59 ft/sec
Reynolds no. Re	181705.58	181705.58	181705.58
Period of a cycle τ	0.05 sec	0.5 sec	0.257 sec
Strouhal no. N_S	0.35	0.35	0.35
Time ratio	1	10	5
Force F	368383.3 lbf	3839.725 lbf	4100.62 lbf
Mass m	2855 lbm	3161.575 lbm	143.577 lbm
N_F	0.1935	0.1935	0.1935

K = 0.357 means that the simulated size is only 35.7% of the prototype size.

The reason for considering full scale simulation is that the prototype may be obtained from the existing recoil mechanism in use without the need of constructing a new simulating model. The use of the same hydraulic fluid in the simulation means that the simulation is identical to the full scale firing of a weapon which is difficult to perform in the laboratory. On the other hand, if simulation with actual size but with water as media is considered, velocity is one-tenth of the actual speed and the time scale is 10 times larger for the simulation and the simulated recoil force $(B)_s$ is reduced ti ibe-hundredth of the real recoil force $(B)_p$. The simulated mass remains the same as that of the prototype. Therefore, the full size simulation with water as hydraulic oil offers advantages of (1) slower simulation velocity, (2) longer simulation time and (3) smaller simulated recoil force. If the full size simulation is still undesirable because of its dimension or of its large mass, the simulation with reduced size is calculated and tabulated in Table 4.

IV. TWO DIMENSIONAL FLOW IN RECOIL MECHANISMS -- A FINITE DIFFERENTIAL METHOD

IV-1. The Finite Differential (FT) Method

In the 1978 annual report [10] of the project and a subsequent report [11], the finite difference solution of unsteady flow in a recoil mechanism was given for a Reynolds number of 3470. Here the Reynolds number was defined with the maximum velocity of the recoil motion and the gap between the cylinder and the recoil rod. The result showed that the finite difference solution with a grid size of (20 x 50) at Reynolds number of 5 is stable but the solution is unstable at the Reynolds number of 3470 and needs a scheme that averages the vorticity solution to stabilize the numerical result. The numerical solution thus only qualitatively agrees with the experimental visualization of the streamline pattern in the upper chamber (the high pressure side) of the recoil mechanism. Further survey of finite difference methods found that the finite difference solution of the Navier-Stokes equation is quite unstable at the high Reynolds number unless the grid size is greatly reduced. Approximately, the grid size Δx required for a stable solution is proportional to the inverse of the Reynolds number. The increase in the number of grids at high Reynolds number requires considerably large computer storage and computational time. Even so, most of finite difference methods show considerable instability if the right combination of parameters such as the time step, the relaxation factor and the method of solving simultaneous equation were not adopted. This difficulty also persists in many simpler flow configurations such as a transient or a steady flow in a square cavity. For this reason, a new numerical method

called the finite differential (FT) method was conceived and developed. The finite differential (FT) method is not the finite difference (FC) method, nor the finite element (FE) method. The basic principle of the finite differential (FT) method is outlined here and then the finite differential (FT) solution for the flow in the square cavity is demonstrated. A better convergence and stability of the numerical solutions are obtained from the finite differential (FT) method.

IV-2. The Principle of Finite Differential (FT) Method

The basic idea of the FT method is the incorporation of local analyti· solutions in the numerical solution of partial differential equation (PDE). The FT method starts with subdivision of the total flow region, D, into small subregions as shown in Figure 8 in which the governing partial differential equation (PDE) may be solved analytically. The assembly of all the local analytic solutions thus constitutes the numerical solution of the problem. Details of the FT method are outlined below.

Consider a partial differential equation, (PDE) with a inhomogeneous term G, $L(\phi) = G$, where L can be any partial differential operator, linear or nonlinear. This PDE is to be solved in a region D, see Figure 1. Depending on the operator L, let the boundary conditions and/or initial conditions be specified so that the problem is well posed. A numerical solution is sought when the problem cannot be solved analytically. In order to solve the problem with the finite differential method, the complex geometry of the problem is broken up into a number of subregions

where analytic solutions can be obtained. Let the region D be subdivided into small rectangles by passing orthogonal lines through the region. The intersection of these lines forms the nodal points with I = 1,2,3,..., i-1, i, i + 1,..., IN, and J = 1,2,3,..., J-1, j, j + 1,...,JN. A typical subregion of the problem with the node point P(i, j) may be surrounded by the neighboring node points E (east), W (west), S (south), N (north), NE (northeast), NW (northwest), SE (southeast) and SW (southwest), which corresponds to points (i + 1, J), (i - 1, j), (i, j - 1), (i, j + 1), (i + 1, j + 1), (i - 1, j + 1), (i + 1, j - 1) and (i - 1, j - 1), respectively.

Once the region D has been subdivided into simple rectangular subregions, an analytic solution in the single subregion may be obtained. In the case when the PDE is nonlinear, the nonlinear equation may be locally linearized in the simple region. However, the overall nonlinear effect can still be preserved by the assembly of local analytic solutions which constitute the numerical solution of the PDE over the whole region D. Indeed, the local linearization technique is also used both in the FC and the FE methods.

The problem has now been reduced into one with many finite regions, where analytic solutions can be obtained if the boundary and initial conditions in each simple finite subregion are properly specified, thereby making each simple subproblem well posed.

Let the governing equation in a simple subregion be $L(\phi) = G$, where L here denotes a linear partial differential operator so that an analytic solution can be obtained for the subregion as a function of the boundary conditions;

$$L(\phi) = G \tag{4-1}$$

$$\phi = f(f_N(x,t),\ f_S(x,t),\ f_E(y,t),\ f_W(y,t),\ h,\ k,\ x,\ y,\ t,\ G) \tag{4-2}$$

where the f_N,f_S,f_E and f_W are prespectively the northern, southern, eastern and western boundary conditions of the subregion. h is the distnce between the point P and the sides N and S. Similarly k is the respective distances between point P and the sides E and W. The boundary conditions f_N and f_S of the element are functions of x, while f_E and f_W are functions of y. The boundary functions f's (i.e., f_N,f_S,f_E and f_W) may be approximately expressed in terms of the nodal values along the boundary such as, f's = $f(\phi_n,\cdots)$ where ϕ_n, are the values of the dependent variables on each node points n, n being E, W, N, S, NE, NW, SE and SW in this particular case. Substituting the boundary conditions expressed by ϕ_n into Eq. (4-2) and evaluating the relationship between the functional value at an interior point of the local subregion p and its surrounding points we have

$$\phi_P = f(\phi_E,\phi_W,\phi_N,\phi_S,\phi_{NE},\phi_{NW},\phi_{SE},\phi_{SW},\cdots) \tag{4-3}$$

which is the fundamental formula for the present FT method. For the linear or locally linearized problem, the 9-point FT formula has the form,

$$\phi_p = C_E\phi_E + C_W\phi_W + C_N\phi_N + C_S\phi_S + C_{NE}\phi_{NE} + C_{SE}\phi_{SE} + C_{NW}\phi_{NW} + C_{SW}\phi_{SW} + S(G) \tag{4-4}$$

where the coefficients C's are obtained from the local analytic solution. S(G) is a part of the inhomogeneous solution. If the larger subregion

shown by the dotted lines in Figure 1 is used, a more accurate 17-point formula can be obtained. It should be remarked here that the finite differential solution obtained in Eq. (4-4) in the interior of the subregion is exact in the sense that it is obtained from an analytical solution to the PDE in the finite subregion. The only approximation involved is from the boundary conditions.

In an internal finite subregion of the total region D, the neighboring points of ϕ_p such as ϕ_E, ϕ_W, etc. are, in general, unknown. However, they can be in turn expressed as an analytic function of their neighboring points. This may be done repeatedly for all the unknown nodes (I,J) in the total region D

$$\phi_{i,j} = C_{i+1,j}\,\phi_{i+1,j} + C_{i-1,j}\,\phi_{i-1,j} + \ldots + f_{i,j}(G) \qquad (4\text{-}5)$$

where $\phi_{i,j}$ is ϕ_p of a given subregion and other ϕ's in Eq. (4-5) are the boundary values given in Eq. (4-4). The assembly of all the expressions for all nodes points can then be expressed in a matrix form. The system of algebraic equations can now be solved numerically as in the finite difference method to give the numerical solution of the total problem. This is the essence of the finite differential (FT) method.

There is an essential difference between the finite differential (FT) method just described and the finite difference (FC) or finite element (FE) methods. In the FC method, the relationship of ϕ_p to its neighboring points is not obtained from the analytic solution of the differential equation but, instead, from the difference formula truncated from the Taylor series expansion of the dependent variable about its neighboring points. On the other hand, the FE method assumes an approximated functional form (shape function), normally some polynomial of lower degree, say up to 5th or 6th degree, to represent the solution and uses

the variational or Galerkin type of integration on the differential equation to find the relation between ϕ_p and its neighboring points. It should be remarked here that the derivatives of the solution from the finite differential solution may be obtained by differentiating Eq. (4-1). The resulting equation will provide the derivative at any given point in the subregion without loss of accuracy due to differentiation.

IV-3. The Finite Differential Solution of Unsteady Two-Dimensional Namier-Stoke Equation

The unsteady two-dimensional incompressible viscous flow can be formulated with the stream function ψ and the vorticity ξ, as a dependent variable. The independent variables are two dimensionless space coordinates (x,y) and the dimensionless time t. These independent variables are normalized with a reference length L and a reference time scale L/U, where U is the reference velocity. The Reynolds number thus is defined as UL/ν. ν is the kinematic viscosity. In order that the stream function satisfies the continuity equation, we have the velocity components in an x and y direction, u and v, as

$$u = \psi_y \quad v = -\psi_x \quad . \tag{4-6}$$

The scalar component of vorticity (z direction) ξ can be defined as

$$\xi = v_x - u_y = -(\psi_{xx} + \psi_{yy}) \quad . \tag{4-7}$$

Taking the curl operation of the momentum equation, we have the voriticy transport equation

$$\xi_t + 2A\xi_x + 2B\xi_y = \xi_{xx} + \xi_{yy} \tag{4-8}$$

with

$$A = R_e\, u/2 \qquad \text{and} \qquad R_e\, v/2 \quad .$$

With the appropriate boundary and initial condition equations (4-6), (4-7), and (4-8) will provide the solutions to u, v, ψ and ξ. The pressure distribution P can be obtained from the integration of the Navier-Stokes equation.

Since equation (4-8) is a nonlinear equation, the analytic solution to the whole region of flow, either in a cavity or in a recoil mechanism is not available. Therefore, the finite differential (FT) numerical solution is one way to obtain an approximate solution. To implement the FT method, the flow region D (see Fig. 4) is subdivided into many subregions. In each region, equation (4-8) is linearized; that is, A and B are assumed as known averaged values within the subregion. In each subregion, the boundary conditions at the north, south, east and west are denoted as $\psi_n, \psi_s, \psi_e, \psi_w$, and $\xi_n, \xi_s, \xi_e, \xi_w$. If the initial condition for the vorticity ξ is given, the problem in the subregion is well defined and can be solved.

Details of the finite differential solution to the vorticity transport equation (4-8) and Poisson equation (4-7) are given respectively in Appendices A and B.

The finite differential solution for the Poisson equation (4-7) is given in Appendix B, equation (B-16) as

$$\psi_p = \sum_{n=1}^{\infty} = (c_6 + c_2 + c)\ \text{Sin}\ \frac{n\pi}{2} + \sum_{m=1}^{\infty} c_4\ \text{Sin}\ \frac{m\pi}{2} \qquad (4\text{-}9)$$

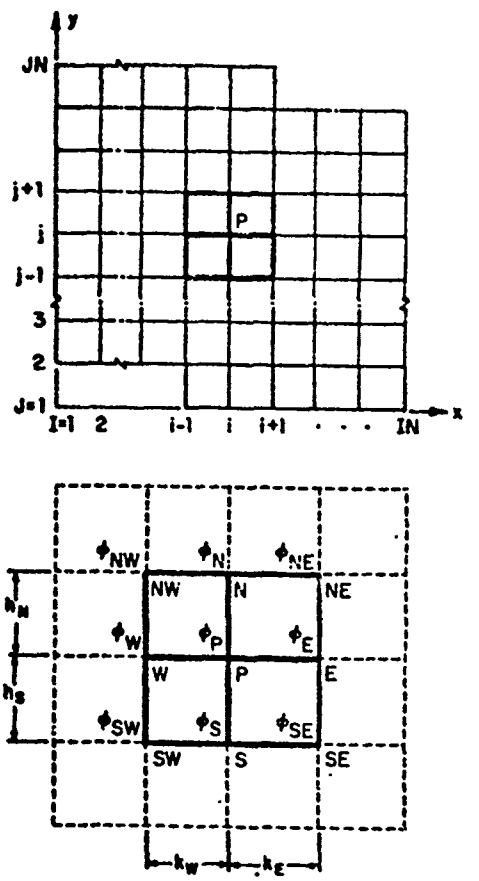

Figure 8. Subregions of the Finite Differential Method

The velocity components u and v may be obtained by differentiation of the stream function ψ. Nine-point formulas for u_p and v_p are given by equations (B-17) and (B-18) of Appendix B.

The coefficients c_2, c_4, c_6, and c are given in Appendix B. They contain the known vorticity in the subregion and the 8-nodal point boundary stream functions (i.e., $\psi_{ne}, \psi_e, \psi_{se}, \psi_n, \psi_{nw}, \psi_w \psi_{sw}$ and ψ_s). Equation (4-9) is thus reduced to the form given in equation (4-4) or, more generally, equation (4-5) relating the central nodal value to the neighboring 8 nodal values.

The steady flow solution of the vorticity transport equation (4-8) is solved to provide the FT 9-point formula for the vorticity at the center of the subregion $\xi_p^s = \xi_p^s(0,0)$ (see Appendix A, equation (A-12)):

$$\xi_p^s = \sum_{n=1}^{\infty} (c_1 + c_2) \operatorname{Sin} \frac{n\pi}{2} + \sum_{m=1}^{\infty} (c_3 + c_4) \operatorname{Sin} \frac{m\pi}{2} \qquad (4\text{-}10)$$

Again, equation (4-10) may be written in the form given by equation (4-4) and (4-5).

IV-4. Numerical Calculation and Discussion

In order to examine the accuracy and stability of the new Finite Differential Method, the case of steady recoil motion without orifice is considered. This is the case similar to the steady state driven cavity flow. The reason for selecting this flow is that there is an abundance of similar works available for comparison.

To solve the steady flow without orifice as shown in Figure 9, equations (4-6), (4-7) and (4-8) must be solved with the boundary conditions

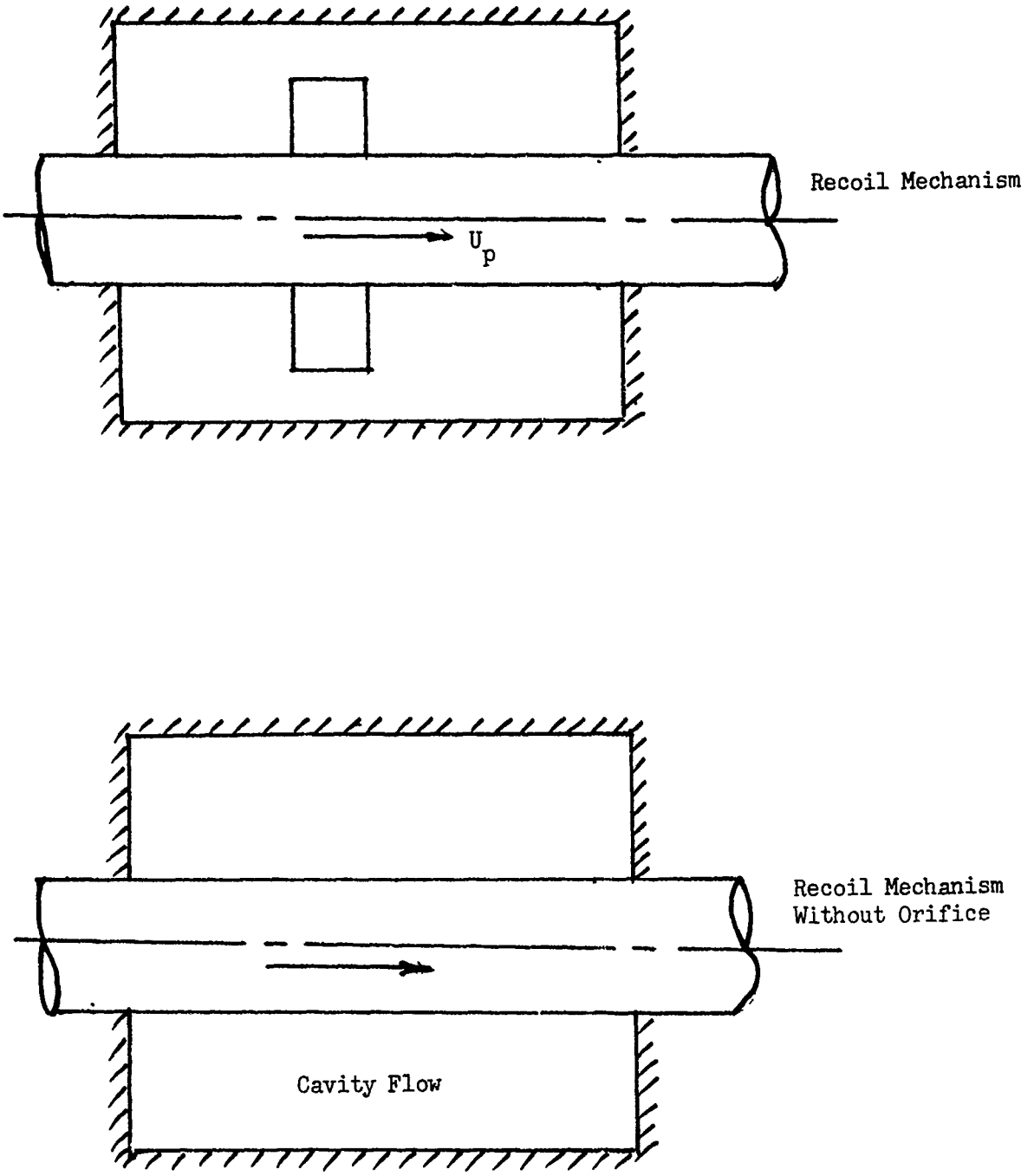

Figure 9 Cavity Flow and Recoil Mechanism

$$
\begin{aligned}
&x = 0 \text{ and } x = 1 \quad , \quad u = v = 0 \text{ or } \psi = 0 \quad , \quad \partial\psi/\partial x = 0 \\
&y = 0 \quad , \quad u = 1, \quad v = 0 \text{ or } \psi = 0 \quad \partial\psi/\partial y = 1 \qquad (4\text{-}11) \\
&y = 1 \quad , \quad u = v = 0 \text{ or } \psi = 0 \quad , \quad \partial\psi/\partial y = 0
\end{aligned}
$$

The finite differential solution of the problem is solved with the finite differential 9-point formulas (4-9) and (4-10) for the stream function and vorticity function. Equations (B-17) and (B-18) in Appendix B provide the finite differential solutions to the velocity components u and v. The numerical solution procedure is as follows:

(1) A guessed vorticity is made and the stream function is solved from equation (4-9) with the boundary condition $\psi = 0$ given in equation (4-11).

(2) The velocity components u and v at each node are calculated from equation (4-10) with the boundary condition (4-11).

(3) The vorticity function is then solved from equation (4-10) with the boundary condition (4-11).

(4) The newly computed vorticity function is compared with the guessed or old vorticity given in Step 1. The solution converges if the difference is within the given convergence criterion. If not, the procedure is repeated from Step (1) using the newly calculated vorticity as the guessed value.

The above procedure is essentially an iterative scheme. In solving each equation, (4-9) and (4-10) an ADI (Alterative Direction Implicit) method is used with the SOR (Succession Over Relaxation) scheme. Also, before returning to Step 1, the SUR scheme is used to reduce the sensitivity of the system of the algebraic equations. Before calculating the

cavity flow problem a test was made to solve a simple problem with constant velocity u and v (i.e., assuming A and B in equation (4-8) to be constant). It was found that the FT solution is more accurate than the finite difference method. In particular, the FT method showed to be more stable than the finite difference method at high Reynolds number (i.e., large value of A and B). For the solution at high Reynolds number, the FT method provides converged solutions when the grid size is reduced. The Reynolds number of 100, 400, and 1,000 have been calculated. As an example, the cavity flow with Re = 1000 is given in Figures 10 and 11. Figure 10 provides the stream pattern of the steady flow in the recoil mechanism without orifice. Figure 11 gives the corresponding vorticity distribution in the cavity.

IV-5. Conclusion

In this chapter, the new numerical method entitled "The Finite Differential Method" is introduced. The finite differential (FT) method is shown to give more accurate results than the finite difference (FC) method under the same flow conditions. Specifically, the convergence and the stability of the FT method is much superior than the FC method.

For the flow with high Reynolds number of the order 10^3 the FT method may still predict stable solution provided that small grid sizes are used and the successive under relaxation (SUR) scheme is used between interactions.

Although the FT method requires much analytic work in the initial derivation of the finite differential formula, the many flow calculation can be solved relatively easily afterward since the finite differential formula are similar even for different flow conditions. The FT method

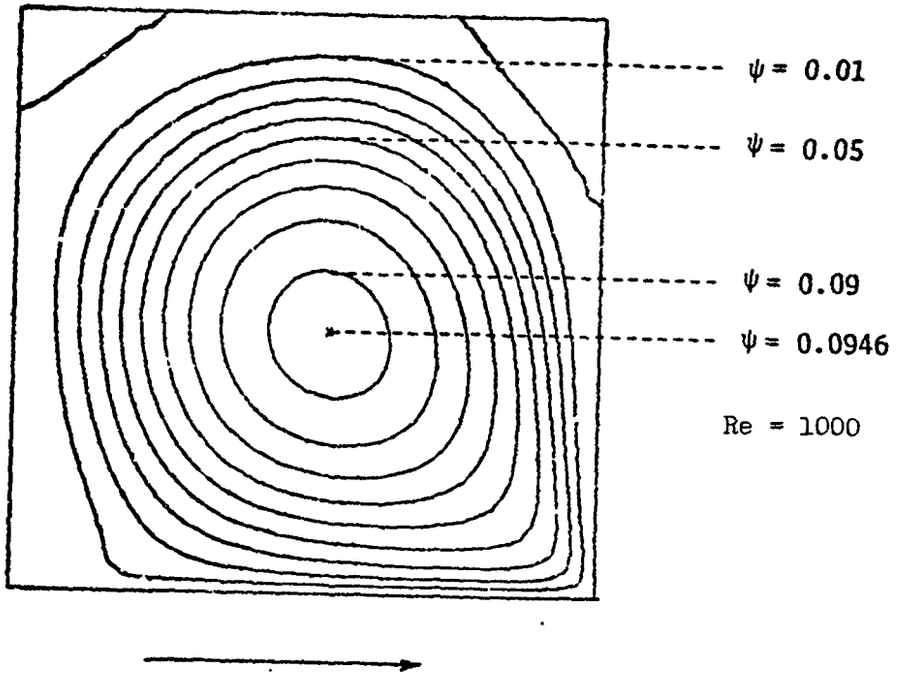

Figure 10 Stream Pattern in Cavity

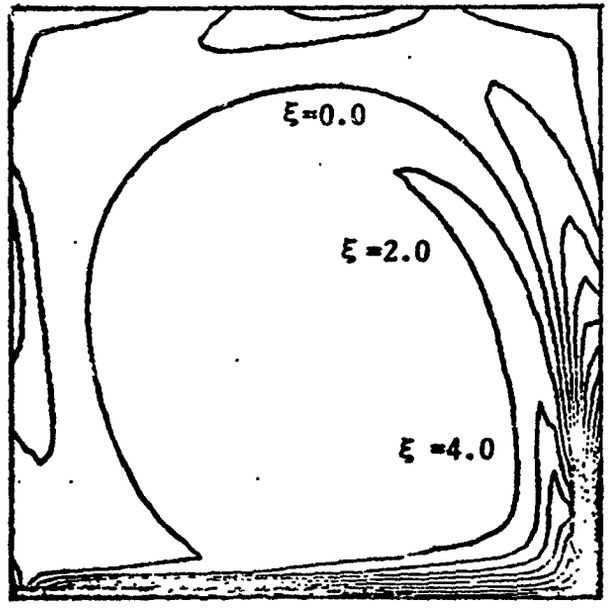

Re = 1000

Figure 11 Vorticity Distrubition in Cavity

is just developed and requires further study before it may put into practical prediction of the orifice coefficient c_d for design of recoil mechanism.

V. SUMMARY, CONCLUSION AND SUGGESTIONS

The present art of the design of recoil mechanisms still relies heavily on the one dimensional analysis of flow motion in the recoil system and on the trial and error method of experiment. The present report attempts to improve the one dimensional fluid flow analysis in Chapter II where the unsteadiness of the flow in record mechanism is approximately incorporated into the use of the orifice discharge coefficient. On the other hand, a simulation design is given in Chapter III where an analysis is given to show how the experimental duration may be increased based on similarity argument, thereby providing a longer time duration for the instrumental measurement as well as the flow visualization. It should be pointed out that the physical understanding of the fluid motion in the recoil mechanism is still lacking. For example, design engineers still do not know when and where the flow in the record mechanism will become turbulent.

In Chapter IV, a new numerical method is developed with the aim to calculate fluid motion at high Reynolds number in the record system. The preliminary calculation shows that the FT method is superior to the FC method in the accuracy of the convergence and the convergence and the stability of the numerical prediction. It is hoped that the design of recoil mechanism may eventually be done first on the computer. Simulation before an expensive experiment and the long duration of the experimentation commences. The modernization of the design of the fluid type recoil mechanism needs the accurate solution of the fluid flow inside the recoil mechanism. In order to achieve this and it requires a commitment of the Army Armament Research and Development Command.

References

[1] Arora, J. S. and Haug, E. J., Jr., "A Guide to Design of Artillery Recoil Mechanisms," Technical Report, Materials Division, College of Engineering, The University of Iowa, Iowa City, IA., July 1977.

[2] Coberly, R. H., "Miscellaneous Artillery Problems," RIA Technical Note, No. 68-288, U.S. Army Weapons Command, Rock Island Arsenal, Rock Island, Illinois, 1968, pp. 1-7.

[3] Moody, B., "Mathematical Computer Simulation of Compressible Fluid Behavior in Recoil Application (Orifice Design)," Army Weap . ; Command Technical Note SWERR-T-TTN-2-72, April 1972.

[4] Frantz, J. W., "Design of New Control Orifices for the M109 E1 155 MM Self-Propelled Howitzer," Technical Report RE-71-9, Science and Technology Laboratory, U.S. Army Weapons Command, March 1971.

[5] Nerdahl, M. C. and Frantz, J. W., "Modeling Effective Fluid Compressibility in a Pateaux Recoil Mechanism," Artillery Weapons Systems Div., SWERR-TR-72-34, Rock Island Arsenal, June 1972.

[6] Coberly, R. H. and Frantz, J. W., "First Approximation of Fluid Flow in Recoil System Specifically Applied to the XM37 Recoil Mechanism," Technical Report No. 16-65, Research and Engineering Division, Rock Island Arsenal, November 1965.

[7] Chen, C. J. and Macagno, E., "Fluid and Thermodynamic Characteristics of Compressible Recoil Mechanism," Technical Report, Energy Division, College of Engineering, The University of Iowa, Iowa City, IA., December 1977.

[8] Lichtarowitz, A, Duggins, R. K. and Markland, E., "Discharge Coefficients for Incompressible Non-Cavitating Flow Through Long Orifice," Journal of Mechanical Engineering Science, Vol. 7, No. 2, 1965, pp. 210-219.

[9] Engineering Design Handbook: Carriage and Mount Series, Record Systems, AMCP, 706-342, U.S. Army Material Command, Washington, D.C. September 1963.

[10] Chen, C. J. "Fluid Mechanics and Thermodynamics of Recoil Mechanics," U.S. Army Armament Research and Development Command. Dover, N.J. Report. Energy Division, The University of Iowa, Iowa City, Iowa 52242, July 1978.

[11] Chen, C. J. Macaguo, E. O. and Chang, K. Y. and Naseri-Neshat" Investigation of Fluid Motion in a Recoil Mechanism" A technical report, Iowa Institute of Hydraulic Research. The University of Iowa. Iowa City, Iowa. 52242 August, 1978.

APPENDIX A. THE 9-POINT FINITE DIFFERENTIAL SOLUTION OF THE VORTICITY TRANSPORT EQUATION

With $A = \frac{1}{2} R_e u$ and $B = \frac{1}{2} R_e v$ assumed to be known constants in a given subregion, the linearized vorticity transport equation for a two dimensional incompressible viscous flow is

$$\xi_t + 2A\,\xi_x + 2B\,\xi_y = \xi_{xx} + \xi_{yy} \tag{A-1}$$

The initial condition or any condition for the next time incremental step in a subregion may be approximately taken as

$$\xi(x,y,t = \bar{\bar{a}}_o + \bar{\bar{a}}_1 y + \bar{\bar{a}}_2 x + \bar{\bar{a}}_3 xy + \bar{\bar{a}}_4 y^2 + \bar{\bar{a}}_5 x^2 + \bar{\bar{a}}_6 xy^2 + \bar{\bar{a}}_7 x^2 y + \bar{\bar{a}}_8 x^2 y^2 \tag{A-2}$$

where 9 coefficients $\bar{\bar{a}}_i (i = 1,1,2,\ldots,8)$ can be determined from the 9 nodal values of ξ at the boundary.

The boundary condition of the subregion may be approximately taken as, for example,

$$\xi_E(y,t) = [(a_E + \bar{a}_E t) + (b_E + \bar{b}_E t)y + (c_E + \bar{c}_E t)y^2] \tag{A-3}$$

Similarly for ξ_S, ξ_N and ξ_W.

Introducing a change of variable

$$\xi = \bar{\xi}\, e^{Ax+By}$$

we may reduce Eq. (A-1) to a simpler form

$$\bar{\xi}_t + (A^2 + B^2)\bar{\xi} = \bar{\xi}_{xx} + \bar{\xi}_{yy} \tag{A-5}$$

with the initial and boundary conditions

$$\text{I.C.} \quad t = t_o \qquad \bar{\xi} = \xi(x,y,t_o)\, e^{-(Ax+By)}$$

$$\text{B.C.} \quad x = \Delta x \qquad \bar{\xi} = \xi_E(y,t)\, e^{-(A\Delta x+By)}$$

$$x = -\Delta x \qquad \bar{\xi} = \xi_W(y,t)\, e^{(A\Delta x-By)} \qquad \text{(A-6)}$$

$$y = \Delta y \qquad \bar{\xi} = \xi_N(x,t)\, e^{-(Ax+B\Delta y)}$$

$$y = -\Delta y \qquad \bar{\xi} = \xi_S(x,t)\, e^{(-Ax+B\Delta y)}$$

The problem of (A-2) with (A-6) may be solved by superposition of a steady part $\bar{\xi}^s$ and an unsteady part $\bar{\xi}^t$, or

$$\bar{\xi} = \bar{\xi}^s(x,y) + \bar{\xi}^t(x,y,t) \qquad \text{(A-7)}$$

or

$$\xi = \xi^s(x,y) + \xi^t(x,y,t)$$

For the FT 9-point formula which provides an algebraic relation between the central node (x = 0, y = 0) value ξ_p with the neighboring 8-point node value Eq. (A-7) can be evaluated at x = 0, y = 0. Details of the derivation of the 9-point formula is given below.

A-1. Solution to the Navier-Stokes Equation, Steady Part

The steady part of the two-dimensional vorticity transport equation now becomes

$$\bar{\xi}^s_{xx} + \bar{\xi}^s_{yy} - (A^2 + B^2)\bar{\xi}^s = 0 \qquad \text{(A-8)}$$

with boundary conditions

$$\bar{\xi}^s = \xi^s_E(y)\, e^{-(A\Delta x+By)} \quad , \qquad x = \Delta x$$

$$\bar{\xi}^s = \xi^s_W(y)\, e^{A\Delta x-By} \quad , \qquad x = -\Delta x$$

$$\bar{\xi}^s = \xi^s_N(x)\, e^{-(ax+B\Delta y)} \quad , \qquad y = \Delta y \tag{A-9}$$

$$\bar{\xi}^s = \xi^s_S(x)\, e^{-As+B\Delta y} \quad , \qquad y = -Ay$$

This problem can be solved analytically by further dividing it into simpler problems having one or two nonhomogenous boundary conditions in one direction. Due to linearity, the final solution will be the superposition of all these simple problems. Assuming a second order polynomial (higher order polynomials can also be taken) for boundaries ξ^s_E, ξ^s_W, ξ^s_N and ξ^s_S, the coefficients can be found in terms of the surrounding vorticities. For example, for the east boundary for the 9-point finite differential (steady part of Eq. (A-3))

$$\xi^s_E(y) = a_E + b_E y + c_E y^2 \tag{A-10}$$

where

$$a_E = \xi_{i+1,j}$$

$$b_E = \frac{1}{2\Delta y}\left(\xi_{i+1,j+1} - \xi_{i+1,j-1}\right)$$

$$c_E = \frac{1}{2\Delta y^2}\left(\xi_{i+1,j+1} - 2\xi_{i+1,j} + \xi_{i+1,j-1}\right)$$

Note should be taken that if only a steady problem is being solved, the vorticities in the above coefficients are the same vorticities as being calculated. However, for the case of unsteady Navier-Stokes equation, the vorticities in these coefficients a_E, b_E and c_E are the previous time step vorticities. In this case the unsteady solution is only part of the overall solution which is added to the unsteady part. If the problem is calculated from fluid at rest, the contribution of the steady part for the first time step will be zero.

The steady vorticity transport Eq. (A-8) is now divided into two simpler problems each with two nonhomogenous boundary conditions as follow:

Problem (1)

$$L\bar{\xi}_1 = 0 \tag{A-11}$$

B.C. $$\bar{\xi}_1 = (a_E + b_E y + c_E y^2)\, e^{-(A\Delta x + By)}, \qquad x = \Delta x$$

$$\bar{\xi}_1 = (a_W + b_W y + c_W y^2)\, e^{A\Delta x - By}, \qquad x = -\Delta x \tag{A-12}$$

$$\bar{\xi}_1 = 0, \qquad y = \pm\Delta y$$

Problem (2)

$$L\bar{\xi}_2 = 0 \tag{A-13}$$

B.C. $$\bar{\xi}_2 = 0, \qquad x = \pm\Delta x$$

$$\bar{\xi}_2 = (a_N + b_N x + c_N x^2)\, e^{-(Ax + B\Delta y)}, \qquad y = \Delta y \tag{A-14}$$

$$\bar{\xi}_2 = (a_S + b_S x + c_S x^2)\, e^{-Ax + B\Delta y}, \qquad y = -\Delta y$$

where

$$\bar{\xi}^s = \bar{\xi}_1 + \bar{\xi}_2$$

and

$$L = \frac{\partial^2}{\partial x^2} + \frac{\partial}{\partial y^2} - (A^2 + B^2)$$

Solution to Problem (1)

Assuming $\bar{\xi}_1^s = X(x)\, Y(y)$, and substituting in the differential equation, the variables are separated. The two boundary conditions in the y-direction in this case are used to find the eigenvalues. Then the problem is reduced to find the function $A_n(x)$ in the series solution

$$\bar{\xi}_1^s(x,y) = \sum_{n=1}^{\infty} A_n(x) \sin \frac{n\pi}{2\Delta y} (y + \Delta y) \qquad \text{(A-15)}$$

To do this, the above equation is differentiated with respect to x and y and substituted in the governing differential equation (A-11) to produce an ordinary differential equation for $A_n(x)$ or

$$A_n''(x) - (A^2 + B^2 + \lambda_n^2)A_n(x) = 0 \qquad \text{(A-16)}$$

When λ_n is the eigenvalue $n\pi/2\Delta y$. The two nonhomogenous boundary conditions in the x-direction are now used to find the solution for this equation.

The solution to Problem (1) becomes

$$\bar{\xi}_1^s(x,y) = \sum_{n=1}^{\infty} (c_1 e^{Ex} + c_2 e^{-Ex}) \sin \frac{n\pi}{2\Delta y} (y + \Delta y) \qquad \text{(A-17)}$$

where

$$C_1 = \frac{A_n(\Delta x)e^{E\Delta x} - A_n(-\Delta x)e^{-E\Delta x}}{e^{2E\,x} - e^{-2E\,x}}$$

$$C_2 = \frac{A_n(-\Delta x)e^{E\Delta x} - A_n(\Delta x)e^{-E\Delta x}}{e^{2E\,x} - e^{-2E\,x}} \qquad \text{(A-18)}$$

with

$$A_n(\Delta x) = \frac{e^{-A\Delta x}}{\Delta y}\,(a_E E_1 + b_E E_2 + c_E E_3)$$

$$A_n(-\Delta x) = \frac{e^{A\Delta x}}{\Delta y}\,(a_W E_1 + b_W E_2 + c_W E_3) \qquad \text{(A-19)}$$

$$E = \sqrt{A^2 + B^2 + \lambda_n^2}$$

and

$$E_1 = \int_{-\Delta y}^{\Delta y} e^{-By} \sin\frac{n\pi}{2\Delta y}\,(y + \Delta y)dy$$

$$E_2 = \int_{-\Delta y}^{\Delta y} y e^{-By} \sin\frac{n\pi}{2\Delta y}\,(y + \Delta y)dy \qquad \text{(A-20)}$$

$$E_3 = \int_{-\Delta y}^{\Delta y} y^2 e^{-By} \sin\frac{n\pi}{2\Delta y}\,(y + \Delta y)dy$$

Solution to Problem (2)

The same procedure as in Problem (1) is repeated for Problem (2) in Eqs. (A-13) and (A-14)

$$\bar{\xi}_2^s = \sum_{m=1}^{\infty} (c_3\, e^{Fy} + c_4\, e^{-Fy}) \sin \frac{m\pi}{2\Delta x} (x + \Delta x) \qquad \text{(A-21)}$$

where

$$F = \sqrt{A^2 + B^2 + \mu_m^2}\ , \qquad \mu_m = \frac{m\pi}{2\Delta x}$$

c_3 and c_4 are similar to c_1 and c_2 with x, Δx, y, Δy, A, and B replaced by y, Δy, x, Δx, B, and A respectively.

Adding Eqs. (A-7) and (A-21) and evaluating at x = 0 and y = 0, we get the central nodal value of teh steady vorticity solution as

$$\xi_p^s = \sum_{n=1}^{\infty} (c_1 + c_2) \sin \frac{n\pi}{2} + \sum_{m=1}^{\infty} (c_3 + c_4) \sin \frac{m\pi}{2} \qquad \text{(A-22)}$$

The neighboring 8 nodal values of vorticity are included in the coefficients c_1, c_2, c_3, and c_4 as given in Eq. (A-18)

A-2. Solution to Unsteady Navier-Stokes Equation

From Eq. (A-7) the problem (A-5) and (A-6), after subtraction of the steady part (A-8) and (A-9), is reduced to

$$L\bar{\xi}^t = 0 \qquad \text{(A-23)}$$

and the initial and boundary conditions become

$$\text{I.C.} \qquad t = t_o \qquad \bar{\xi}^t = \xi^{n-1}(x,y,t_o)\, e^{-(Ax+By)} \qquad \text{(A-24)}$$

$$\text{B.C.} \qquad x = \Delta x \qquad \bar{\xi}^t = \xi_E(y,t)\, e^{-(A\Delta x+By)}$$

$$x = -\Delta x \qquad \bar{\xi}^t = \xi_W(y,t)\, e^{+A\Delta x-By}$$

$$y = \Delta y \qquad \bar{\xi}^t = \xi_N(x,t)\ e^{-(Ax+B\Delta y)}$$

$$y = -\Delta y \qquad \bar{\xi}^t = \xi_S(x,t)\ e^{-Ax+B\Delta y} \tag{A-25}$$

where

$$L = \frac{\partial}{\partial t} - \frac{\partial^2}{\partial x^2} - \frac{\partial^2}{\partial y^2} + (A^2 + B^2)$$

In order to solve the time dependent problem (A-23) with given boundary and initial conditions (A-24) and (A-25), it is divided into five simpler problems each having one nonzero boundary or initial condition. These are given as follows:

Problem (3):

$$L\tilde{\xi}_0 = 0$$

$$\text{I.C.} \quad \tilde{\xi}_0 = \xi^{n-1}(x,y)\ e^{-(Ax+By)}\ , \qquad t = t_0 = 0$$

$$\text{B.C.} \quad \tilde{\xi}_0 = 0\ , \qquad x = \pm\Delta x \tag{A-26}$$

$$\tilde{\xi}_0 = 0\ , \qquad y = \pm\Delta y$$

Problem (4):

$$L\tilde{\xi}_1 = 0\ ,$$

$$\text{I.C.} \quad \tilde{\xi}_1 = 0\ , \qquad t = 0$$

$$\text{B.C.} \quad \tilde{\xi}_1 = (a_E t + b_E ty + c_E ty^2)\ e^{-(A\Delta x+By)}\ , \qquad x = \Delta x \tag{A-27}$$

$$\tilde{\xi}_1 = 0\ , \qquad x = -x$$

$$\tilde{\xi}_1 = 0\ , \qquad y = y$$

Problem (5):

$$L\tilde{\xi}_2 = 0$$

I.C. $\tilde{\xi}_2 = 0$, $t = 0$

B.C. $\tilde{\xi}_2 = 0$, $x = \Delta x$ (A-28)

$\tilde{\xi}_2 = (\bar{a}_W t + \bar{b}_W ty + c_W ty^2)\, e^{A\Delta x - By}$, $x = -\Delta x$

$\tilde{\xi}_2 = 0$, $y = \pm\Delta y$

Problem (6):

$$L\tilde{\xi}_3 = 0$$

I.C. $\tilde{\xi}_3 = 0$, $t = 0$

B.C. $\tilde{\xi}_3 = 0$, $x = \pm\Delta x$ (A-29)

$\tilde{\xi}_3 = (\bar{a}_N t + \bar{b}_N ty + \bar{c}_N ty^2)\, e^{A\Delta x - By}$, $y = \Delta y$

$\tilde{\xi}_3 = 0$, $y = -\Delta y$

Problem (7):

$$L\tilde{\xi}_4 = 0$$

I.C. $\tilde{\xi}_4 = 0$, $t = 0$

B.C. $\tilde{\xi}_4 = 0$, $x = \pm\Delta x$ (A-30)

$\tilde{\xi}_4 = 0$, $y = \Delta y$

$\tilde{\xi}_4 = (\bar{a}_S t + \bar{b}_S tx + \bar{c}_S tx^2)\, e^{-As + B\Delta y}$, $y = -\Delta y$

In the above problems, the coefficients $\bar{a}$, $\bar{b}$, and $\bar{c}$ are given in terms of the boundary vorticity. For example, for the east boundary;

$$\bar{a}_E = \xi_{i+1,j}/\Delta t$$

$$\bar{b}_E = (\xi_{i+1,j+1} - \xi_{i+1,j-1})/2\Delta t\Delta y \qquad \text{(A-31)}$$

$$\bar{c}_E = (\xi_{i+1,j+1} - 2\xi_{i+1,j} + \xi_{j+1,j-1})/?\Delta t\Delta y^2$$

Solution to Problem (3)

Because of the linearization (assumption of constant A and B in a subregion), the variables can be separated and solved accordingly. The vorticity $\xi^{n-1}(x,y)$ in the initial condition is just the value of vorticity in the subregion at initial time (previous time step is denoted by a superscript n-1) which can be approximated by a polynomial of x and y. For a 9-point finite differential, the polynomial and the coefficients are:

$$\xi^{n-1}(x,y) = \bar{\bar{a}}_0 + \bar{\bar{a}}_1 y + \bar{\bar{a}}_2 x + \bar{\bar{a}}_3 xy + \bar{\bar{a}}_4 y^2 + \bar{\bar{a}}_5 x^2 + \bar{\bar{a}}_6 xy^2 + \bar{\bar{a}}_7 x^2 y + \bar{\bar{a}}_8 x^2 y^2 \qquad \text{(A-32)}$$

where

$$\bar{\bar{a}}_0 = \xi^{n-1}_{i,j}$$

$$\bar{\bar{a}}_1 = \frac{1}{2\Delta y}\left(\xi^{n-1}_{i,j+1} - \xi^{n-1}_{i,j-1}\right)$$

$$\bar{\bar{a}}_2 = \frac{1}{2\Delta x}\left(\xi^{n-1}_{i+1,j} - \xi^{n-1}_{i-1,j}\right)$$

$$\bar{\bar{a}}_3 = \frac{1}{4\Delta x\Delta y}\left(\xi^{n-1}_{i+1,j+1} + \xi^{n-1}_{i-1,j-1} - \xi^{n-1}_{i-1,j+1} - \xi^{n-1}_{i+1,j-1}\right)$$

$$a_4 = \frac{1}{2\Delta y^2}\left(\xi^{n-1}_{i,j+1} + \xi^{n-1}_{i,j-1} + 2\xi^{n-1}_{i,j}\right)$$

$$\bar{a}_5 = \frac{1}{2\Delta x^2}\left(\xi^{n-1}_{i+1,j} + \xi^{n-1}_{i-1,j} + 2\xi^{n-1}_{i,j}\right)$$

$$\bar{a}_6 = \frac{1}{4\Delta x\Delta y^2}\left(\xi^{n-1}_{i+1,j+1} - \xi^{n-1}_{i-1,j-1} - \xi^{n-1}_{i-1,j+1} + \xi^{n-1}_{i+1,j-1} - 2\xi^{n-1}_{i+1,j} + 2\xi^{n-1}_{i-1,j}\right)$$

$$\bar{a}_7 = \frac{1}{4\Delta x^2\Delta y}\left(\xi^{n-1}_{i+1,j+1} + \xi^{n-1}_{i-1,j+1} - \xi^{n-1}_{i+1,j-1} - \xi^{n-1}_{i+1,j-1} - 2\xi^{n-1}_{i,j+1} + 2\xi^{n-1}_{i,j-1}\right)$$

$$\bar{a}_8 = \frac{1}{4\Delta x^2\Delta y^2}\left(\xi^{n-1}_{i+1,j+1} + \xi^{n-1}_{i-1,j+1} + \xi^{n-1}_{i+1,j-1} + \xi^{n-1}_{i-1,j-1} - 4\xi^{n-1}_{i,j} - 2\xi^{n-1}_{i,j+1} - 2\xi^{n-1}_{i,j-1} - 2\xi^{n-1}_{i+1,j} - 2\xi^{n-1}_{i-1,j}\right) \quad \text{(A-33)}$$

The analytic solution to Problem (3) is found to be

$$\tilde{\xi}_0 = \sum_{k=1}^{\infty}\sum_{\ell=1}^{\infty}\left\{e^{-\eta t} - 1 + \frac{1}{\Delta x\Delta y}\left[H - \Delta y(c_1Q_1 + c_2Q_2) - \Delta x(c_3Q_3 + c_4Q_4)\right]\right\} \times \sin\frac{k\pi}{2}\sin\frac{\ell\pi}{2} \quad \text{(A-34)}$$

where

$$\eta = A^2 + B^2 + \left(\frac{k\pi}{2\Delta x}\right)^2 + \left(\frac{\ell\pi}{2\Delta y}\right)^2$$

$$H = \bar{\bar{a}}_0E_1'\bar{E}_1' + \bar{\bar{a}}_1E_2'\bar{E}_1' + \bar{\bar{a}}_2E_1'\bar{E}_2' + \bar{\bar{a}}_3E_2'\bar{E}_2' + \bar{\bar{a}}_4E_3'\bar{E}_1' + \bar{\bar{a}}_5E_1'\bar{E}_3' + \bar{\bar{a}}_6E_3'\bar{E}_2' + \bar{\bar{a}}_7E_2'\bar{E}_3' + \bar{\bar{a}}_8E_3'\bar{E}_3'$$

$$\bar{E}_1' = \int_{-\Delta y}^{\Delta y} e^{-By}\sin\frac{\ell\pi}{2\Delta y}(y + \Delta y)dy$$

$$\bar{E}_2' = \int_{-\Delta y}^{\Delta y} ye^{-By}\sin\frac{\ell\pi}{2\Delta y}(y + \Delta y)dy$$

$$\bar{E}_3' = \int_{-\Delta y}^{\Delta y} y^2 \, e^{-By} \sin \frac{\ell\pi}{2\Delta y} (y + \Delta y) dy \qquad \text{(A-35)}$$

E_1', E_2' and E_3' are similar to $\bar{E}_1'$, $\bar{E}_2'$ and $\bar{E}_3'$ respectively with y, Δy, B and ℓ changed to x, Δx, A and k.

c_1, c_2, c_3 and c_4 are the same as the steady part. Q_1 and Q_2 are

$$Q_1 = e^{-E\Delta x} \left\{ \frac{\frac{k\pi}{2\Delta x} [1 - (-1)^k \, e^{2E\Delta x}]}{E^2 + \left(\frac{k\pi}{2\Delta x}\right)^2} \right\}$$

$$Q_2 = e^{E\Delta x} \left\{ \frac{\frac{k\pi}{2\Delta x} [1 - (-1)^k \, e^{-2E\Delta x}]}{E^2 + \left(\frac{k\pi}{2\Delta x}\right)^2} \right\}$$

$$E = \sqrt{A^2 + B^2 + \left(\frac{\ell\pi}{2\Delta x}\right)^2}$$

Again Q_3 and Q_4 are similar to Q_1 and Q_2 with Δx and k changed to Δy and ℓ respectively.

Solution to Problem (4)

This problem is solved similarly by the method of separation of variables. Assuming $\tilde{\xi}_1 = F(t,x)\ Y(y)$, and substituting into the differential equation (A-27), the variables are separated. The two zero boundary conditions at $y = \pm\Delta y$ are used to find the eigenvalues. Thus the problem is reduced to finding $F_\ell(t,x)$ in

$$\xi_1(x,y,t) = \sum_{\ell=1}^{\infty} F_\ell(t,x) \sin \frac{\ell\pi}{2\Delta y} (y + \Delta y) \qquad \text{(A-36)}$$

To find $F_\ell(t,x)$, first a change of variable is made so that a homogenous boundary condition in the x-direction is found by assuming

$$\bar{F}_\ell = F_\ell - \frac{x + \Delta x}{2\Delta x} \frac{e^{-\cdot\Delta x}}{\Delta y} (\bar{a}_E \bar{E}_1' + \bar{b}_E \bar{E}_2' + \bar{c}_E \bar{E}_3')t \qquad \text{(A-37)}$$

by substitution of Eq. (A-37) into Eq. (A-27) a new nonhomogenous differential equation with the variables t and x will be found with homogenous boundary and initial condition which can be solved again by separation of variables with the result

$$\tilde{\xi}_1 = \sum_{\ell=1}^{\infty} \sum_{k=1}^{\infty} A_{k_1}(t) \sin \frac{k\pi}{2\Delta x} (x + \Delta x) \sin \frac{\ell\pi}{2\Delta y} (y + \Delta y) + \sum_{\ell=1}^{\infty} \frac{x + \Delta x}{2\Delta x} \alpha$$

$$+ \sin \frac{\ell\pi}{2\Delta y} (y + \Delta y) \qquad \text{(A-38)}$$

which can be evaluated at the center of the subregion x = 0 and y = 0. The coefficient $A_{k_1}(t)$ is

$$A_{k_1}(t) = \frac{1}{\eta} \left(t - \frac{1}{\eta} + \frac{e^{-\eta t}}{\eta} \right) \gamma + \frac{1}{\eta} (1 - e^{-\eta t}) \delta$$

where

$$\eta = A^2 + B^2 + \left(\frac{\ell\pi}{2\Delta y}\right)^2 + \left(\frac{k\pi}{2\Delta x}\right)^2$$

$$\gamma = - \frac{\alpha}{2\Delta x^2} \left[A^2 + B^2 + \left(\frac{\ell\pi}{2\Delta y}\right)^2 \right] Pk1$$

$$\delta = - \frac{\alpha}{2\Delta x^2} \; Pk1$$

$$Pk1 = -2\Delta x(-1)^k / \left(\frac{k\pi}{2\Delta x}\right)$$

$$\alpha = \frac{e^{-A\Delta x}}{\Delta y} \left(\bar{a}_E \bar{E}_1' + \bar{b}_E \bar{E}_2' + \bar{c}_E \bar{E}_3'\right) \tag{A-39}$$

$$\bar{a}_E = \frac{1}{\Delta t} \xi_{i+1,j}$$

$$\bar{b}_E = \frac{1}{2\Delta t \Delta y} \left(\xi_{i+1,j+1} - \xi_{i+1,j-1}\right)$$

$$\bar{c}_E = \frac{1}{2\Delta t \Delta y^2} \left(\xi_{i+1,j+1} - 2\xi_{i+1,j} + \xi_{i+1,j-1}\right)$$

Solution to Problem (5)

The solution procedure for this problem is similar to Problem (4) but only the nonhomogenity is changed from the position $x = \Delta x$ to $x = -\Delta x$. The solution is

$$\tilde{\xi}_2 = \sum_{\ell=1}^{\infty} \sum_{k=1}^{\infty} A_{k_2}(t) \sin \frac{k\pi}{2\Delta x} (x + \Delta x) \sin \frac{\ell\pi}{2\Delta y} (y + \Delta y)$$

$$- \sum_{\ell=1}^{\infty} \frac{x - \Delta x}{2\Delta x} \sin \frac{\ell\pi}{2\Delta y} (y + \Delta y) \tag{A-40}$$

where

$$A_{k_2}(t) = \frac{1}{\eta} \left(t - \frac{1}{\eta} + \frac{e^{-\eta t}}{\eta}\right) \gamma + \frac{1}{\eta} (1 - e^{-\eta t}) \delta$$

$$\eta = A^2 + B^2 + \left(\frac{\ell\pi}{2\Delta y}\right)^2 + \left(\frac{k\pi}{2\Delta x}\right)^2$$

$$\gamma = \frac{\alpha}{2\Delta x^2} \left[A^2 + B^2 + \left(\frac{\pi\ell}{2\Delta y}\right)^2\right] Pk2$$

$$\delta = \frac{\alpha}{2\Delta x^2} \, Pk2$$

$$Pk2 = -\frac{4\Delta x^2}{k\pi}$$

$$\alpha = \frac{e^{A\Delta x}}{\Delta y} \left(\bar{a}_W \bar{E}_1' + \bar{b}_W \bar{E}_2' + \bar{c}_W \bar{E}_3'\right)$$

The solution to Problems (6) and (7) are similar to Problems (4) and (5) with x, Δx, y, Δy, k, ℓ, A and B changing to y, Δy, x, Δx, ℓ, k, B and A respectively. Also the boundaries change respectively from East and West to North and South.

APPENDIX B. THE 9-POINT FINITE DIFFERENTIAL SOLUTION OF THE TWO-DIMENSIONAL POISSON EQUATION

The two-dimensional Poisson equation and its boundary condition here are given as

$$\frac{\partial^2 \psi}{\partial x^2} + \frac{\partial^2 \psi}{\partial y^2} = -\xi(x,z) \tag{B-1}$$

with boundary conditions

$$\begin{aligned} \psi &= \psi_E(y) \quad , \qquad x = \Delta x \\ \psi &= \psi_W(y) \quad , \qquad x = -\Delta x \\ \psi &= \psi_N(x) \quad , \qquad y = \Delta y \\ \psi &= \psi_S(x) \quad , \qquad y = -\Delta y \end{aligned} \tag{B-2}$$

where for the 9-point finite-differential method the boundaries will be second order polynomials of x or y. As an example

$$\psi_E(y) = a'_E + b'_E y + c'_E y^2 \tag{B-3}$$

where

$$a'_E = \psi_{i+1,j}$$

$$b'_E = \frac{1}{2\Delta y} (\psi_{i+1,j+1} - \psi_{i+1,j-1})$$

$$c'_E = \frac{1}{2\Delta y^2} (\psi_{i+1,j+1} - 2\psi_{i+1,j} + \psi_{i+1,j-1})$$

To solve the problem (B-1) and (B-2), it is divided into two simpler problems as

$$\psi = \psi_1 + \psi_2 \tag{B-4}$$

where

Problem (1):

$$\begin{aligned} &\nabla^2\psi_1 = 0 \\ &\psi_1 = \psi_E(y) \quad , \qquad x = \Delta x \\ &\psi_1 = \psi_W(y) \quad , \qquad x = -\Delta x \\ &\psi_1 = \psi_N(x) \quad , \qquad y = \Delta y \\ &\psi_1 = \psi_S(x) \quad , \qquad y = -\Delta y \end{aligned} \tag{B-5}$$

Problem (2):

$$\begin{aligned} &\nabla^2\psi_2 = -\xi(x;y) \\ &\psi_2 = 0 \quad , \qquad x = \pm\Delta x \\ &\psi_2 = 0 \quad , \qquad y = \pm\Delta y \end{aligned} \tag{B-6}$$

B-1. Solution to Problem (1)

Again for simplicity and due to linearity, this problem is divided into two problems each having two homogeneous boundary conditions as:

$$\psi_1(x,y) = u(x,y) + w(x,y) \tag{B-7}$$

where

$$\nabla^2 u = 0$$

$$u = \psi_E(y) \quad , \qquad x = \Delta x$$

$$u = \psi_W(y) \quad , \qquad x = -\Delta x \tag{B-8}$$

$$u = 0 \quad , \qquad y = \pm\Delta y$$

and

$$\nabla^2 w = 0$$

$$w = 0 \quad , \qquad x = \pm\Delta x$$

$$w = \psi_N(x) \quad , \qquad y = \Delta y \tag{B-9}$$

$$w = \psi_S(x) \quad , \qquad y = -\Delta y$$

The solution to u and w can simply be found by separation of variable and added together to give the solution to Problem (1).

$$\psi_1 = \sum_{n=1}^{\infty} [c_1 \sinh(\mu_n x) + c_2 \cosh(\mu_n x)] \sin \frac{n\pi}{2\Delta y} (y - \Delta y)$$

$$+ \sum_{m=1}^{\infty} [c_3 \sinh(\mu_m y) + c_4 \cosh(\mu_m y)] \sin \frac{m\pi}{2\Delta x} (x + \Delta x) \tag{B-10}$$

where

$$C_1 = \frac{(a'_E - a'_w)E'_1 + (b'_E - b'_w)E'_2 + (c'_E - c'_w)E'_3}{2\Delta y \sinh(\mu_n \Delta x)}$$

$$C_2 = \frac{(a'_E + a'_w)E'_1 + (b'_E + b'_W)E'_2 + (c'_E + c'_w)E'_3}{2\Delta y \sinh(\mu_n \Delta x)}$$

and

$$\mu_n = \frac{n\pi}{2\Delta y} \quad , \qquad \mu_m = \frac{m\pi}{2\Delta x}$$

c_3 and c_4 are similar to c_1 and c_2 but x, Δx, y, Δy, a and B are replaced with y, Δy, x, Δx, B and A respectively.

B-2. Solution to Problem (2)

In this case first the homogenous equation is solved and with the use of two homogenous boundary conditions, the eigenvalues are found. The solution to Problem (2) given by Eq. (B-6) is assumed to be

$$\psi_2(x,y) = \sum_{m=1}^{\infty} c_n(x) \sin \frac{n\pi}{2\Delta y} (y + \Delta y) \tag{B-11}$$

To find the unknown function $c_n(x)$, Eq. (B-11) is substituted into the Poisson equation (B-6) resulting in

$$\sum_{m=1}^{\infty} [c_n''(x) - \mu_n^2 c_n(x)] \sin \mu_n(y + \Delta y) = -\xi(x,y) \tag{B-12}$$

Now the vorticity $\xi(x,y)$ can be assumed to be a polynomial of x and y related to the 9-nodal points in the finite differential element. The coefficients of the polynomial are thus expressed by the 9-nodal values of the vorticity. Now that $\xi(x,y)$ is known it can be expanded in terms of Fourier sine series and substitued in Eq. (B-12). On setting the coefficients of the sine terms on each side equal to each other, a second order ordinary differential equation for $c_n(x)$ will result which can be solved accordingly. The homogenous boundary conditions in the y-direction can now be used to find the two constants of integration. The result of

Problem (2) thus becomes

$$\psi_2 = \sum_{n=1}^{\infty} [c_5 \sinh(\mu_n x) + c_6 \cosh(\mu_n x) + ax^2 + bx + c] \sin \frac{n\pi}{2\Delta y} (y + \Delta y) \tag{B-13}$$

$$c_5 = - \frac{b\Delta x}{\sinh(\mu_n \Delta x)}$$

$$c_6 = - \frac{c + \Delta x^2 a}{\cosh(\mu_n \Delta x)}$$

$$a = \frac{1}{\mu_n^2 \Delta y} (\bar{\bar{a}}_5 E_1' + \bar{\bar{a}}_6 E_2' + \bar{\bar{a}}_9 E_3') \tag{B-14}$$

$$b = \frac{1}{\frac{2}{n} y} (\bar{\bar{a}}_2 E_1' + \bar{\bar{a}}_4 E_2' + \bar{\bar{a}}_8 E_3')$$

$$c = \frac{1}{\mu_n^2 \Delta y} (\bar{\bar{a}}_1 E_1' + \bar{\bar{a}}_3 E_2' + \bar{\bar{a}}_7 E_3') + \frac{2}{\mu_n^2} a$$

$$\mu_n = \frac{n\pi}{2\Delta y}$$

Note that $\bar{\bar{a}}$'s are evaluated at the present vorticity values if the flow under consideration is an unsteady flow.

In this part E_1', E_2', and E_3' are

$$E_1' = \int_{-\Delta y}^{\Delta y} \sin \frac{n\pi}{2\Delta y} (y + \Delta y) dy$$

$$E_2' = \int_{-\Delta y}^{\Delta y} y \sin \frac{n\pi}{2\Delta y} (y + \Delta y) dy \tag{B-15}$$

$$E_3' = \int_{-\Delta y}^{\Delta y} y^2 \sin \frac{n\pi}{2\Delta y} (y + \Delta y) dy$$

The FT 9-point formula for the stream function, ψ, thus is obtained by superposing the solutions, ψ_1 and ψ_2, given in Eqs. (B-10) and (B-13), and evaluating them at the center of the subregion x = 0, y = 0, or $\psi_p(0.0)$

$$\psi_p = \psi_1(0.0) + \psi_2(0.0)$$

$$= \sum_{n=1}^{\infty} -c_2 \sin \frac{n\pi}{2} + \sum_{m=1}^{p} c_4 \sin \frac{m\pi}{2}$$

$$+ \sum_{n=1}^{\infty} (c_6 + c) \sin \frac{n\pi}{2} \qquad \text{(B-16)}$$

The velocity components $u = \partial\psi/\partial y$ and $v = -\partial\psi/\partial x$ are obtained by the differentiation of the stream function ψ_1 and ψ_2 given in Eqs. (B-10) and (B-13) with respect to x and y. Thus the velocity components at the center node of the subregion $u_p = u(0.0)$, $v = v(0.0)$ are

$$u_p = \frac{\partial\psi_1}{\partial y} + \frac{\partial\psi_2}{\partial y}$$

$$= \sum_{n=1}^{\infty} c_2 \mu_n \cos \frac{n\pi}{2\Delta y} + \sum_{m=1}^{\infty} c_3 \mu_m \sin \frac{m\pi}{2}$$

$$+ \sum_{n=1}^{\infty} [c_6 + c] \mu_n \cos \frac{n\pi}{2} \qquad \text{(B-17)}$$

$$v_p = - \left(\frac{\partial \psi_1}{\partial x} + \frac{\partial \psi_2}{\partial x} \right)$$

$$= - \sum_{n=1}^{\infty} c_1 \mu_n \sin \frac{n\pi}{2} - \sum_{m=1}^{\infty} c_4 \mu_m \cos \frac{m\pi}{2}$$

$$- \sum_{n=1}^{\infty} [c_5 \mu_n + b] \sin \frac{n\pi}{2} \qquad \text{(B-18)}$$